JOURNAL OF COMPUTATIONAL PHYSICS 107, 262–281 (1993)

Dispersion-Relation-Preserving Finite Difference Schemes for Computational Acoustics

CHRISTOPHER K. W. TAM AND JAY C. WEBB

Department of Mathematics, Florida State University, Tallahassee, Florida 32306-3027

Received February 18, 1992; revised September 14, 1992

Acoustics problems are governed by the linearized Euler equations. According to wave propagation theory, the number of wave modes and their wave propagation characteristics are all encoded in the dispersion relations of the governing equations. Thus one is assured that the numerical solutions of a high order finite difference scheme will have the same number of wave modes (namely, the acoustic, vorticity, and entropy waves), the same wave propagation characteristics (namely, nondispersive, nondissipative, and isotropic) and the same wave speeds as those of the solutions of the Euler equations if both systems of equations have the same dispersion relations. Finite difference schemes which have the same dispersion relations as the original partial differential equations are referred to as dispersion-relation-preserving (DRP) schemes. A way to construct time marching DRP schemes by optimizing the finite difference approximations of the space and time derivatives in the wave number and frequency space is proposed. The stability of these schemes is analyzed and a sufficient condition for numerical stability is established. A set of radiation and outflow boundary conditions compatible with the DRP schemes is constructed. These conditions are derived from the asymptotic solutions of the governing equations. The asymptotic solutions are found by the use of Fourier–Laplace transforms and the method of stationary phase. A sequence of numerical simulations has been carried out. These simulations are designed to test the effectiveness of the DRP schemes and the radiation and outflow boundary conditions. The computed solutions agree very favorably with the exact solutions. The radiation boundary conditions perform satisfactorily causing little acoustic reflections. The outflow boundary conditions are found to be quite transparent to outgoing disturbances even when the disturbances are made up of a combination of acoustic, vorticity, and entropy waves.

1. INTRODUCTION

Most current computational fluid dynamics (CFD) finite difference schemes are designed for the solution of time independent problems. In the formulation of these schemes the requirements of consistency and numerical stability are imposed. By invoking the Lax equivalence theorem the convergence of these schemes is then assured. The quality of CFD schemes is generally ranked by the order of (Taylor series) truncation. It is expected that a fourth-order scheme is better than a second-order scheme and so on. For time independent problems the above criteria are quite sufficient. Great progress has been made over the years in the application of CFD methods to aerodynamics and aircraft design problems (see Refs. [1–9]).

For time dependent problems, especially acoustics problems, a consistent, stable, and convergent high order scheme does not guarantee a good quality numerical wave solution. A simple analysis of the linearized compressible Euler equations reveals that in a uniform mean flow the partial differential equations support three types of waves, namely, the acoustic, the entropy, and the vorticity waves. The acoustic waves are isotropic, nondispersive, nondissipative and propagate with the speed of sound. The entropy and vorticity waves are nondispersive, nondissipative, and highly directional. They propagate (convected) in the direction of the mean flow with the same speed as the flow. There is no guarantee in most of the popular CFD schemes that the finite difference equations support waves with these characteristics. In fact, many current CFD codes are dispersive, anisotropic, and even highly dissipative (sometimes artificial dissipation terms are deliberately added to improve numerical stability, e.g., Ref. [4]). Thus by using existing CFD codes for acoustics computations one is certain of obtaining a numerically stable solution but whether the solution (for finite Δx, Δy) adequately simulates the wave solution of the governing partial differential equations is an open question.

The main objective of this paper is to present a new optimized high order finite difference scheme which not only meets the usual conditions of consistency, stability, and hence convergence but also supports, in the case of small amplitude waves, wave solutions which have (as nearly as possible) the same characteristics as those of the linearized Euler equations. A second objective of this paper is to present a set of radiation and outflow boundary conditions which are compatible with the proposed high order finite difference scheme.

It is well known in wave propagation theory (e.g., Whitham [10]) that the propagation characteristics of the waves governed by a system of partial differential equations

0021-9991/93 $5.00

are encoded in the dispersion relation in the frequency and wave number space. The dispersion relation is a functional relation between the angular frequency of the waves and the wave numbers of the spatial variables. This relation is usually obtained by taking the space and time Fourier transforms of the governing equations. The dispersiveness, damping rate, isotropy or anisotropy, group and phase velocities of all the waves supported by the medium governed by the partial differential equations are all determined by the dispersion relation. With this understanding it is clear that what is needed is a finite difference scheme which has the same or almost the same dispersion relation as the original partial differential equations. In a discretized system a minimum of five mesh points is needed to define a period of a sine wave. Hence the above statement needs only to be true for waves with wave numbers α, β such that $\alpha \Delta x$, $\beta \Delta y \leqslant \pi/2$ (i.e., waves with wavelengths greater than or equal to four mesh spacings), where Δx and Δy are the mesh sizes in the x and y directions, respectively. This class of finite difference schemes will be referred to as dispersion-relation-preserving (DRP) schemes.

In developing finite difference approximation of partial derivatives the standard way is to use a truncated Taylor series. But from the wave propagation point of view this is not necessarily the best way. If the motivation is to preserve the dispersion relation then the finite difference approximation should be constructed so that the Fourier transform is preserved. In other words, it would be desirable to have a finite difference scheme with nearly the same Fourier transform in space or time as the original partial derivative. Obviously this step is crucial to the dispersion-relation-preserving method. Finite difference approximation of the spatial derivatives formulated in this way will be discussed in detail in Section 2. The treatment for the time derivative requires slightly different consideration. It is discussed in Section 4.

High order finite difference schemes invariably introduce extraneous numerical solutions. The nature of these solutions depends strongly on the chosen values of the computational parameters. For numerical stability it is important that the parameter be set to the proper numerical range so that the extraneous solutions are all heavily damped. An analysis of the numerical stability of the DRP schemes is given in Section 5. It turns out that the requirement of minimum numerical damping to the physical acoustic wave solution sometimes imposes an even more stringent condition on the size of the time marching step than numerical stability. Numerical damping of the computed solution is often not a critical issue in computational fluid dynamics. However, it is of vital importance to the quality of the solution for acoustics problems. A way to estimate the size of the time step needed to meet a permissible level of degradation of the computed solution by numerical damping is discussed in Section 6.

To ensure good quality global computational acoustic solutions the outer boundaries of the computational domain must be transparent to all outgoing waves. For the linearized Euler equations with a uniform mean flow the acoustic waves are the principal outgoing waves except on the outflow boundary. Along the outflow boundary the outgoing disturbances consist of a combination of acoustic, entropy, and vorticity waves. Hence special outflow boundary conditions are needed to allow the exit of these waves from the computation domain without reflection. For the other boundaries the imposition of a simple acoustic radiation boundary condition is sufficient. Radiation and outflow boundary conditions have been considered by numerous investigators in the past. Bayliss and Turkel [11, 12] developed a family of radiation boundary conditions based on the far field asymptotic solution of the simple wave equation. Engquist and Majda [13, 14] used a pseudo-differential operator technique to construct absorbing boundary conditions. The absorbing boundary condition minimizes the reflected waves off the artificial boundary of the computation domain. This idea has since been refined by Higdon [15, 16] and Jiang and Wong [17]. Kosloff and Kosloff [18] proposed the incorporation of an artificial damping layer as absorbing boundaries for wave propagation problems. Most recently Thompson [19, 20] formulated radiation and outflow boundary conditions by means of the characteristics of the governing partial differential equations. In this work the radiation and outflow boundary conditions are derived from the far field asymptotic solutions of the linearized Euler equations. For disturbances with wavelengths longer than five mesh spacings these conditions are compatible with the numerical solutions of the DRP scheme.

To validate the effectiveness of the DRP scheme and the radiation and outflow boundary conditions proposed in this paper, a sequence of numerical experiments and comparisons with exact solutions of the linearized Euler equations have been carried out. In the numerical experiments reported in detail in Section 8 an acoustic wave pulse is initiated at the center of the computation domain superimposed on a uniform flow. The acoustic disturbance propagates outward at the speed of sound and at the same time it is convected downstream by the mean flow. Downstream of the acoustic pulse an entropy and a vorticity pulse are simultaneously introduced into the flow. The separation distances of the pulses are so arranged that all of them exit the outflow boundary at the same time. This offers a critical test of the outflow boundary conditions. Computation results indicate that the calculated waveforms are in good agreement with the exact solution. There are no noticeable effects of dissipation and dispersion. When the disturbances reach the boundaries of the computation domain only very low amplitude reflected waves can be detected. A clear message from all the computed results

is that the DRP scheme together with the radiation and outflow boundary conditions can be used to provide high quality solutions to computational acoustics problems.

2. OPTIMIZED SPATIAL DISCRETIZATION

Consider the approximation of the first derivative $\partial f/\partial x$ at the lth node of a uniform grid. Suppose M values of f to the right and N values of f to the left of this point are used to form the finite difference approximation, i.e.,

$$\left(\frac{\partial f}{\partial x}\right)_l \simeq \frac{1}{\Delta x}\sum_{j=-N}^{M} a_j f_{l+j}. \tag{2.1}$$

The usual procedure is to expand the right-hand side of (2.1) in Taylor series of Δx and then determine the coefficients a_j by equating coefficients of the same powers of Δx. Finite difference schemes constructed in this way will be referred to as the standard schemes. In this paper the coefficients a_j are to be chosen in a different way. It is proposed that they be determined by requiring the Fourier transform of the finite difference scheme on the right of (2.1) to be a close approximation of that of the partial derivative on the left.

The finite difference equation (2.1) is a special case of the following equation in which x is a continuous variable:

$$\frac{\partial f}{\partial x}(x) \simeq \frac{1}{\Delta x}\sum_{j=-N}^{M} a_j f(x + j\,\Delta x); \tag{2.2}$$

(2.1) can be recovered from (2.2) by setting $x = l\,\Delta x$. The Fourier transform and its inverse of a function are related by

$$\tilde{f}(\alpha) = \frac{1}{2\pi}\int_{-\infty}^{\infty} f(x)\, e^{-i\alpha x}\, dx \tag{2.3a}$$

$$f(x) = \int_{-\infty}^{\infty} \tilde{f}(\alpha)\, e^{i\alpha x}\, d\alpha. \tag{2.3b}$$

The Fourier transform of the left and right sides of (2.2) are

$$i\alpha\tilde{f} \simeq \left(\frac{1}{\Delta x}\sum_{j=-N}^{M} a_j e^{i\alpha j\,\Delta x}\right)\tilde{f}. \tag{2.4}$$

By comparing the two sides of (2.4) it is clear that the quantity

$$\bar{\alpha} = \frac{-i}{\Delta x}\sum_{j=-N}^{M} a_j e^{ij\alpha\,\Delta x} \tag{2.5}$$

is effectively the wave number of the Fourier transform of the finite difference scheme (2.2) or (2.1); $\bar{\alpha}\,\Delta x$ is a periodic function of $\alpha\,\Delta x$ with period 2π. To assure that the Fourier transform of the finite difference scheme is a good approximation of that of the partial derivative over the range of wave numbers of interest (waves with wave length longer than four Δx or $|\alpha\,\Delta x| < \pi/2$) it is required that a_j be chosen to minimize the integrated error E defined

$$E = \int_{-\pi/2}^{\pi/2} |\alpha\,\Delta x - \bar{\alpha}\,\Delta x|^2\, d(\alpha\,\Delta x)$$

$$= \int_{-\pi/2}^{\pi/2} \left| i\kappa - \sum_{j=-N}^{M} a_j e^{ij\kappa} \right|^2 d\kappa. \tag{2.6}$$

The conditions that E is a minimum are

$$\frac{\partial E}{\partial a_j} = 0, \qquad j = -N \text{ to } M; \tag{2.7}$$

(2.7) provides a system of linear algebraic equations by which the coefficients a_j can be easily determined.

The special case of $N = M$ is of particular interest. In this case $\bar{\alpha}$ is real and the right-hand side of (2.5) is a truncated Fourier sine series. In other words, the finite difference scheme tries to approximate the partial derivative by a Fourier sine series in the wave number space. If N and M are not equal (the stencil is unsymmetric) $\bar{\alpha}$ is complex. It can be shown that when such an unsymmetric stencil is used over a large region it will generally lead to spatially growing wave solutions. To avoid this type of numerical instability, in this work, only central difference schemes will be used. Unsymmetric stencils may, however, be employed in limited regions (such as at the boundary regions of the computation domain) without leading to accumulated numerical instability.

It is possible to combine the traditional truncated Taylor series finite difference approximation and the wave number space approximation described above. For instance, if $N = M = 3$ one can impose the condition that (2.2) be accurate to order $(\Delta x)^4$. This leaves one of the coefficients, say a_1, as a free parameter. This parameter can then be chosen to minimize the error integral E of (2.6). When this constrained minimization is carried out, it is straightforward to find that the coefficients are

$$a_0 = 0$$

$$a_1 = -a_{-1} = 0.79926643$$

$$a_2 = -a_{-2} = -0.18941314$$

$$a_3 = -a_{-3} = 0.02651995.$$

Figure 1 shows the relation $\bar{\alpha}\,\Delta x$ and $\alpha\,\Delta x$ over the interval 0 to π, using the above coefficients. For $\alpha\,\Delta x$ up to 1.45 the curve is nearly the same as the straight line $\bar{\alpha} = \alpha$. Thus the

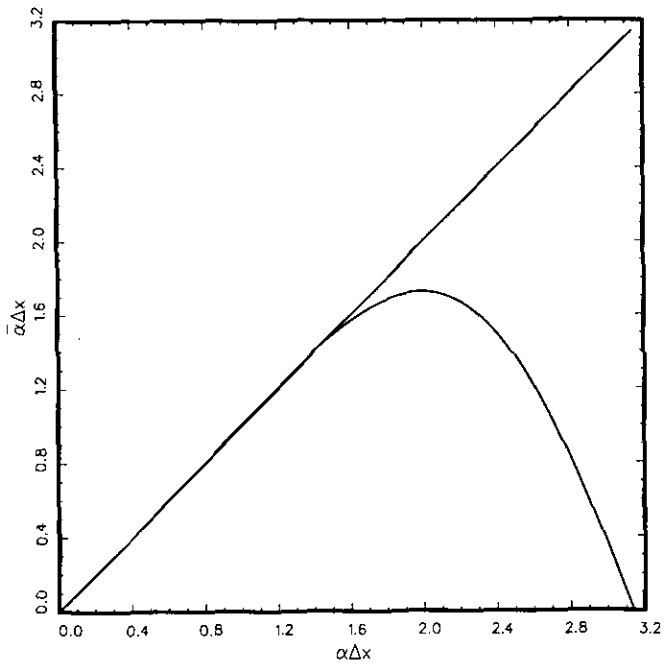

FIG. 1. $\bar{\alpha}\,\Delta x$ versus $\alpha\,\Delta x$ for the optimized fourth-order central finite difference scheme ($N = M = 3$).

finite difference scheme can provide an adequate approximation to the partial derivative for waves with wave lengths longer than 4.5 mesh spacings. For $\alpha\,\Delta x$ greater than 2.0 the $\bar{\alpha}(\alpha)$ curve deviates increasingly from the straight line relationship. Because of this the wave propagation characteristics of the short wave components of the finite difference equations would be very different from those of the partial differential equations.

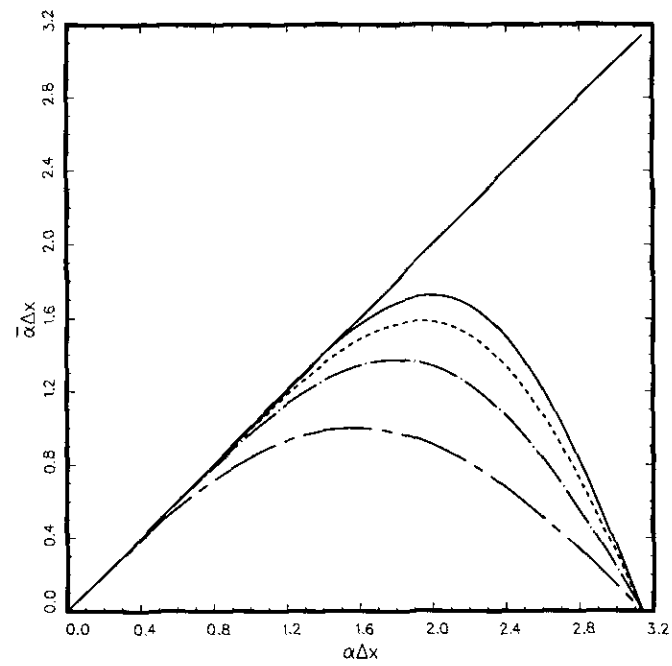

FIG. 2. $\bar{\alpha}\,\Delta x$ versus $\alpha\,\Delta x$: ——— optimized fourth-order scheme; – – – standard sixth-order scheme; —·— standard fourth-order scheme; —— standard second-order scheme.

Figure 2 shows the $\bar{\alpha}\,\Delta x$ versus $\alpha\,\Delta x$ relation for the standard sixth-order ($N = M = 3$, a seven-point stencil) central finite difference scheme. It is easy to see that the curve starts to deviate from the linear relation $\bar{\alpha} = \alpha$ at $\alpha\,\Delta x = 1.0$. In other words, the standard scheme can provide adequate approximation to waves with wave lengths longer than 6.5 mesh spacings. On comparing with the optimized fourth-order scheme it is seen that the latter significantly improves the resolution power of the computation at virtually no additional effort and computing time. Shown in Fig. 2 also are the $\bar{\alpha}\,\Delta x$ versus $\alpha\,\Delta x$ curves for the standard second- (three-point stencil) and fourth- (five-point stencil) order central finite difference schemes. It is easy to find that they give good approximations to the first derivative for $|\alpha\,\Delta x|$ up to 0.4 and 0.8, respectively. This means that they are adequate to resolve waves with wave lengths longer than 16 and 8 mesh spacings, respectively. Thus the use of a high order optimized scheme is necessary in problems involving high frequency (short wave length) waves.

3. DISPERSION RELATIONS AND ASYMPTOTIC SOLUTIONS OF THE LINEARIZED EULER EQUATIONS

Consider small amplitude disturbances superimposed on a uniform mean flow of density ρ_0, pressure p_0 and velocity u_0 in the x-direction. The linearized Euler equations for the disturbances in two dimensions are

$$\frac{\partial \mathbf{U}}{\partial t} + \frac{\partial \mathbf{E}}{\partial x} + \frac{\partial \mathbf{F}}{\partial y} = \mathbf{H} \tag{3.1}$$

where

$$\mathbf{U} = \begin{bmatrix} \rho \\ u \\ v \\ p \end{bmatrix}, \quad \mathbf{E} = \begin{bmatrix} \rho_0 u + \rho u_0 \\ u_0 u + p/\rho_0 \\ u_0 v \\ u_0 p + \gamma p_0 u \end{bmatrix}, \quad \mathbf{F} = \begin{bmatrix} \rho_0 v \\ 0 \\ p/\rho_0 \\ \gamma p_0 v \end{bmatrix}.$$

The nonhomogeneous term $\mathbf{H}$ on the right side of (3.1) represents distributed unsteady sources.

The Fourier–Laplace transform of a function $f(x, y, t)$ (denoted by $\tilde{f}$) and its inverse are related by:

$$\tilde{f}(\alpha, \beta, \omega) = \frac{1}{(2\pi)^3} \int_0^\infty \iint_{-\infty}^{\infty} f(x, y, t) \times e^{-i(\alpha x + \beta y - \omega t)}\, dx\, dy\, dt \tag{3.2}$$

$$f(x, y, t) = \int_\Gamma \iiint_{-\infty}^{\infty} \tilde{f}(\alpha, \beta, \omega)\, e^{i(\alpha x + \beta y - \omega t)} \times d\alpha\, d\beta\, d\omega. \tag{3.3}$$

In (3.3) the contour Γ is a line parallel to the real axis in the complex ω-plane above all the poles and singularities of the integrand.

The general initial value problem of (3.1) for arbitrary nonhomogeneous source term **H** can be solved formally by Fourier–Laplace transforms. On applying Fourier–Laplace transforms to Equation (3.1) the equation for $\tilde{\mathbf{U}}$ becomes

$$\mathbf{A}\tilde{\mathbf{U}} = \tilde{\mathbf{G}}, \tag{3.4}$$

where

$$\mathbf{A} = \begin{bmatrix} (\omega - \alpha u_0) & -\rho_0\alpha & -\rho_0\beta & 0 \\ 0 & (\omega - \alpha u_0) & 0 & -\alpha/\rho_0 \\ 0 & 0 & \omega - \alpha u_0 & -\beta/\rho_0 \\ 0 & -\gamma p_0 \alpha & -\gamma p_0 \beta & \omega - \alpha u_0 \end{bmatrix} \tag{3.4a}$$

and $\tilde{\mathbf{G}} = i(\tilde{\mathbf{H}} + \tilde{\mathbf{U}}_{\text{initial}}/2\pi)$ represents the sum of the transforms of the source term and the initial conditions. It is easy to show that the eigenvalues λ_j and eigenvectors $\mathbf{X}_j$ ($j = 1$, 2, 3, 4) of matrix **A** are

$$\lambda_1 = \lambda_2 = (\omega - \alpha u_0) \tag{3.5}$$

$$\lambda_3 = (\omega - \alpha u_0) + a_0(\alpha^2 + \beta^2)^{1/2} \tag{3.6}$$

$$\lambda_4 = (\omega - \alpha u_0) - a_0(\alpha^2 + \beta^2)^{1/2} \tag{3.7}$$

$$\mathbf{X}_1 = \begin{bmatrix} 1 \\ 0 \\ 0 \\ 0 \end{bmatrix}, \quad \mathbf{X}_2 = \begin{bmatrix} 0 \\ \beta \\ -\alpha \\ 0 \end{bmatrix}, \tag{3.8}$$

$$\mathbf{X}_3 = \begin{bmatrix} \dfrac{1}{a_0^2} \\ \dfrac{-\alpha}{\rho_0 a_0(\alpha^2+\beta^2)^{1/2}} \\ \dfrac{-\beta}{\rho_0 a_0(\alpha^2+\beta^2)^{1/2}} \\ 1 \end{bmatrix}, \quad \mathbf{X}_4 = \begin{bmatrix} \dfrac{1}{a_0^2} \\ \dfrac{\alpha}{\rho_0 a_0(\alpha^2+\beta^2)^{1/2}} \\ \dfrac{\beta}{\rho_0 a_0(\alpha^2+\beta^2)^{1/2}} \\ 1 \end{bmatrix},$$

where $a_0 = (\gamma p_0/\rho_0)^{1/2}$ is the speed of sound. The solution of (3.4) may be expressed as a linear combination of the eigenvectors:

$$\tilde{\mathbf{U}} = \frac{C_1}{\lambda_1}\mathbf{X}_1 + \frac{C_2}{\lambda_2}\mathbf{X}_2 + \frac{C_3}{\lambda_3}\mathbf{X}_3 + \frac{C_4}{\lambda_4}\mathbf{X}_4. \tag{3.9}$$

The coefficient vector **C**, having elements C_j ($j = 1$ to 4), is given by

$$\mathbf{C} = \mathbf{X}^{-1}\tilde{\mathbf{G}}. \tag{3.10}$$

$\mathbf{X}^{-1}$ is the inverse of the fundamental matrix

$$\mathbf{X}^{-1} = \begin{bmatrix} 1 & 0 & 0 & -\dfrac{1}{a_0^2} \\ 0 & \dfrac{\beta}{(\alpha^2+\beta^2)} & -\dfrac{\alpha}{(\alpha^2+\beta^2)} & 0 \\ 0 & -\dfrac{1}{2}\dfrac{\rho_0 a_0 \alpha}{(\alpha^2+\beta^2)^{1/2}} & -\dfrac{1}{2}\dfrac{\rho_0 a_0 \beta}{(\alpha^2+\beta^2)^{1/2}} & \dfrac{1}{2} \\ 0 & \dfrac{1}{2}\dfrac{\rho_0 a_0 \alpha}{(\alpha^2+\beta^2)^{1/2}} & \dfrac{1}{2}\dfrac{\rho_0 a_0 \beta}{(\alpha^2+\beta^2)^{1/2}} & \dfrac{1}{2} \end{bmatrix}; \tag{3.11}$$

(3.9) represents the decomposition of the solution into the entropy wave, $\mathbf{X}_1$, the vorticity wave, $\mathbf{X}_2$, and the two modes of acoustic waves, $\mathbf{X}_3$ and $\mathbf{X}_4$.

According to standard wave propagation theory, e.g., Ref. [10] the dispersion relations of the waves governed by Eq. (3.4) are given by the zeros of the determinant **A**. However, the determinant **A** is zero whenever ω, α, and β are so related that any one of the eigenvalues λ_j ($j = 1$, 2, 3, 4) is equal to zero. Thus the dispersion relations of the waves of the linearized Euler equations can be found by setting the eigenvalues to zero.

3.1. *The Entropy Wave*

The entropy wave consists of density fluctuations alone, i.e., $u = v = p = 0$. The dispersion relation is given by the poles of (3.9) in the transform planes or

$$\lambda_1 = (\omega - \alpha u_0) = 0. \tag{3.12}$$

By inverting the Fourier–Laplace transform, it is straightforward to find that ρ is given by

$$\rho(x, y, t) = \int_\Gamma \iiint_{-\infty}^{\infty} \frac{C_1}{(\omega - \alpha u_0)} e^{i(\alpha x + \beta y - \omega t)} \times d\alpha\, d\beta\, d\omega. \tag{3.13}$$

For large time, $t \to \infty$, the threefold integrals of (3.13) can be evaluated formally (see Appendix A). If the source has a finite duration the formal solution has the form

$$\rho(x, y, t) = \begin{cases} \chi(x - u_0 t, y), & x \to \infty \\ 0, & x \to -\infty. \end{cases} \tag{3.14}$$

Thus the entropy wave is convected downstream by the uniform mean flow without distortion.

3.2. *The Vorticity Wave*

The vorticity wave consists of velocity fluctuations alone. That is, there are no pressure and density fluctuations associated with this wave mode ($p = \rho = 0$). The dispersion relation is given by

$$\lambda_2 = (\omega - \alpha u_0) = 0 \tag{3.15}$$

which is identical to that of the entropy wave. Therefore, the vorticity wave has the same wave propagation characteristics as the entropy wave. By inverting the Fourier–Laplace transforms it is easy to find that for large time the formal solution has the form

$$u(x, y, t) = \begin{cases} \dfrac{\partial \psi}{\partial y}, & x \to \infty \\ 0, & x \to -\infty \end{cases}$$
$$v(x, y, t) = \begin{cases} \dfrac{-\partial \psi}{\partial x}, & x \to \infty \\ 0, & x \to -\infty, \end{cases} \tag{3.16}$$

where $\psi = \psi(x - u_0 t, y)$.

3.3. *The Acoustic Wave*

The acoustic waves involve fluctuations in all the physical variables. The dispersion relation is given by

$$\lambda_3 \lambda_4 = (\omega - \alpha u_0)^2 - a_0^2(\alpha^2 + \beta^2) = 0. \tag{3.17}$$

The formal solution can be found by inverting the Fourier–Laplace transforms. In the far field, that is, in regions away from the sources, the inversion integrals can be evaluated by the method of residues and the method of stationary phase (see Appendix A). The asymptotic solution ($r \to \infty$; r and θ are the polar coordinates) may be written in the form

$$\begin{bmatrix} \rho \\ u \\ v \\ p \end{bmatrix} \sim \frac{F(r/V(\theta) - t, \theta)}{r^{1/2}} \begin{bmatrix} 1 \\ \dfrac{1}{a_0^2} \\ \dfrac{\hat{u}(\theta)}{\rho_0 a_0} \\ \dfrac{\hat{v}(\theta)}{\rho_0 a_0} \\ 1 \end{bmatrix} + O(r^{-3/2}), \tag{3.18}$$

where

$$V(\theta) = u_0 \cos\theta + a_0(1 - M^2 \sin^2\theta)^{1/2}; \qquad M = u_0/a_0$$
$$\hat{u}(\theta) = \frac{\cos\theta - M(1 - M^2 \sin^2\theta)^{1/2}}{(1 - M^2 \sin^2\theta)^{1/2} - M\cos\theta}$$
$$\hat{v}(\theta) = \sin\theta[(1 - M^2 \sin^2\theta)^{1/2} + M\cos\theta];$$

$V(\theta)$ is the effective velocity of propagation in the θ-direction.

4. OPTIMIZED TIME DISCRETIZATION

In this paper the primary interest is on developing an explicit time marching scheme. However, the procedure formulated below may also be used to develop implicit time marching schemes.

The linearized Euler equations (3.1) provide the time derivatives of $\mathbf{U}$. Suppose the solution is known up to a time level $t = n\,\Delta t$. To advance to the next time step a four-level finite difference approximation in the form

$$\mathbf{U}^{(n+1)} - \mathbf{U}^{(n)} \simeq \Delta t \sum_{j=0}^{3} b_j \left(\frac{d\mathbf{U}}{dt}\right)^{(n-j)} \tag{4.1}$$

is proposed. To ensure that the scheme is consistent, three of the four coefficients b_j ($j = 1, 2, 3$) will be chosen so that (4.1) is satisfied to order $(\Delta t)^3$ when both sides are expanded by Taylor series. This leaves one free parameter b_0. The relations between the other coefficients and b_0 are

$$b_1 = -3b_0 + \tfrac{53}{12}, \quad b_2 = 3b_0 - \tfrac{16}{3}, \quad b_3 = -b_0 + \tfrac{23}{12}. \tag{4.2}$$

The remaining coefficient b_0 will now be determined by requiring that the Laplace transform of the above finite difference scheme (4.1) be a good approximation of that of the partial derivative.

The finite difference equation (4.1) is a special case of the difference equation in which t is a continuous variable,

$$\mathbf{U}(t + \Delta t) - \mathbf{U}(t) \simeq \Delta t \sum_{j=0}^{3} b_j \frac{d}{dt}\mathbf{U}(t - j\,\Delta t); \tag{4.3}$$

(4.3) is identical to (4.1) if t is set equal to $n\,\Delta t$. It will be assumed for the time being that $\mathbf{U}$ satisfies the following trivial initial conditions, i.e.,

$$\mathbf{U}(t) = 0, \qquad t < \Delta t. \tag{4.4}$$

The appropriate nonzero initial conditions for the time marching finite difference scheme will be discussed later.

By applying the Laplace transform to (4.3) it is easy to obtain

$$-i\frac{i(e^{-i\omega\Delta t} - 1)}{\Delta t \sum_{j=0}^{3} b_j e^{ij\omega\Delta t}}\,\tilde{\mathbf{U}} \simeq \frac{d\tilde{\mathbf{U}}}{dt}, \tag{4.5}$$

where $\tilde{}$ represents the Laplace transform. The Laplace transform of the time derivative of $\mathbf{U}$, i.e., the right side of

(4.5), is, however, equal to $-i\omega\tilde{U}$. Thus by comparing the two sides of (4.5) the quantity

$$\bar{\omega} = \frac{i(e^{-i\omega\Delta t} - 1)}{\Delta t \sum_{j=0}^{3} b_j e^{ij\omega\Delta t}} \tag{4.6}$$

is the effective angular frequency of the time discretization scheme (4.1). The weighted integral error, E_1, incurred by using $\bar{\omega}$ to approximate ω will be defined by

$$E_1 = \int_{-0.5}^{0.5} \{\sigma[\mathrm{Re}(\bar{\omega}\,\Delta t - \omega\,\Delta t)]^2 + (1-\sigma) \times [\mathrm{Im}(\bar{\omega}\,\Delta t - \omega\,\Delta t)]^2\}\, d(\omega\,\Delta t), \tag{4.7}$$

where σ is the weight on the real part. The value b_0 is chosen to minimize E_1. It is the root of the equation

$$\frac{dE_1}{db_0} = 0. \tag{4.8}$$

As an example, if a weight $\sigma = 0.36$ is used (4.8) gives $b_0 = 2.30255809$. From (4.2) the other coefficients are

$$b_1 = -2.49100760, \qquad b_2 = 1.57434093, \qquad b_3 = -0.38589142. \tag{4.9}$$

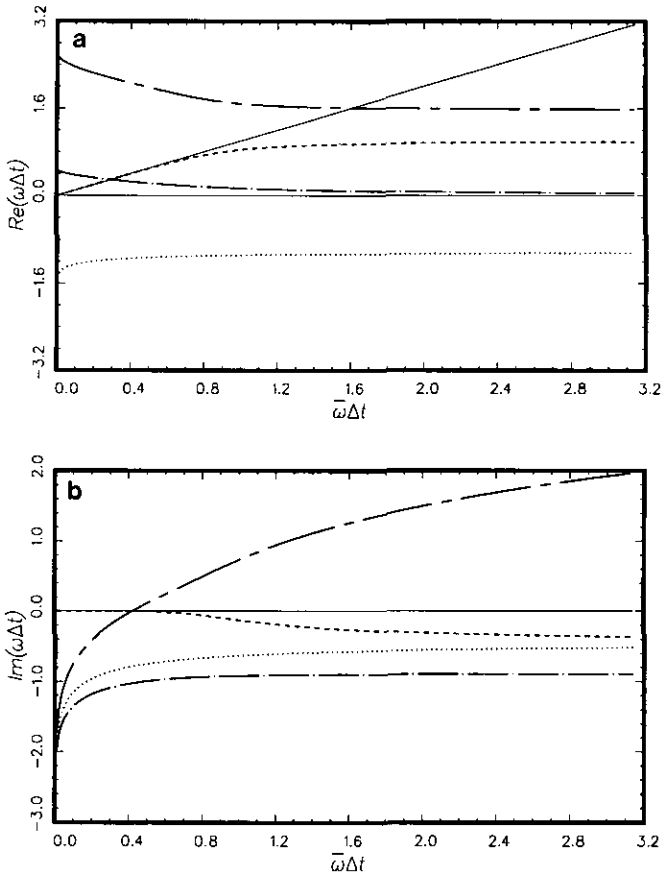

FIG. 3. The dependence of the four roots of $\omega\,\Delta t$ on $\bar{\omega}\,\Delta t$ ($\sigma = 0.36$): (a) real parts; (b) imaginary parts.

The weight σ allows one to adjust the degree of emphasis one wishes to impose on the optimization process in favor of having better wave propagation characteristics (real part of ω) or damping characteristics (imaginary part of ω). The value $\sigma = 0.36$ appears to be a well-balanced choice.

The relationship between $\bar{\omega}$ and ω is not one to one. This means that the finite difference marching scheme (4.1) will contain spurious numerical solutions. It is easy to see that for a given $\bar{\omega}\,\Delta t$ there are four values of $\omega\,\Delta t$ which satisfy (4.6). Figures (3a) and (3b) show the dependence of the real and imaginary parts of these roots on $\bar{\omega}\,\Delta t$ over the range $0 \leqslant \bar{\omega}\,\Delta t < \pi$ using the coefficients of (4.9). For negative values of $\bar{\omega}$ the values of ω may be found by the extension formula

$$\omega(-\bar{\omega}) = -\omega^*(\bar{\omega}) \tag{4.10}$$

(* indicates the complex conjugate) which is implicit in (4.6). It is to be noted that three of the roots have negative imaginary parts over the entire range of $\bar{\omega}\,\Delta t$ shown. The fourth root has negative imaginary part only for $\bar{\omega}\,\Delta t < 0.4$. For larger values of $\bar{\omega}\,\Delta t$ the imaginary part of this root becomes positive. It will be shown later that this spurious root could cause numerical instability if too large a time step is used.

A closer examination of Fig. 3 reveals that only the root with nearly zero imaginary part gives a good approximation to the desired straightline relation $\bar{\omega} = \omega$ over a limited range of $\bar{\omega}\,\Delta t$ ($\bar{\omega}\,\Delta t < 0.6$; note the optimized range in (4.7) has accordingly been chosen to be from -0.5 to 0.5). To ensure that the dispersion relation of the wave modes supported by the finite difference scheme are close approximations of the corresponding wave modes of the Euler equations, the values of $\omega\,\Delta t$ in the entire computation must be restricted to the range of -0.6 to 0.6.

5. STABILITY OF DISPERSION-RELATION-PRESERVING SCHEMES

It will now be shown that by applying the optimized spatial discretization scheme of Section 2 and the optimized time discretization scheme of Section 4 to the linearized Euler equations (3.1) a DRP finite difference scheme is obtained. Let the $x-y$ plane be divided into a mesh of spacings Δx and Δy in the x and y directions, respectively.

It is easy to find that the discretized form of (3.1) is (for the $N = M = 3$ case)

$$\mathbf{K}_{l,m}^{(n)} = -\frac{1}{\Delta x}\sum_{j=-3}^{3} a_j \mathbf{E}_{l+j,m}^{(n)} - \frac{1}{\Delta y}\sum_{j=-3}^{3} a_j \mathbf{F}_{l,m+j}^{(n)} + \mathbf{H}_{l,m}^{(n)} \tag{5.1}$$

$$\mathbf{U}_{l,m}^{(n+1)} = \mathbf{U}_{l,m}^{(n)} + \Delta t \sum_{j=0}^{3} b_j \mathbf{K}_{l,m}^{(n-j)}, \tag{5.2}$$

where l, m are the indices of the mesh points and n is the time level. If $\mathbf{U} = \mathbf{U}_{\text{initial}}$ at $t = 0$ is the initial conditions for the Euler equations, the appropriate initial conditions for the finite difference marching scheme (5.1)–(5.2) is

$$\mathbf{U}_{l,m}^{(0)} = \mathbf{U}_{\text{initial}}, \qquad \mathbf{U}_{l,m}^{(n)} = 0 \text{ for negative } n. \tag{5.3}$$

To find the dispersion relations of the above finite difference scheme consider the generalized form of these equations with continuous variables. The complete problem consists of the following equations and initial conditions:

$$\mathbf{K}(x, y, t) = -\frac{1}{\Delta x}\sum_{j=-3}^{3} a_j \mathbf{E}(x + j\,\Delta x, y, t) - \frac{1}{\Delta y}\sum_{j=-3}^{3} a_j \mathbf{F}(x, y + j\,\Delta y, t) + \mathbf{H}(x, y, t) \tag{5.4}$$

$$\mathbf{U}(x, y, t + \Delta t) = \mathbf{U}(x, y, t) + \Delta t \sum_{j=0}^{3} b_j \mathbf{K}(x, y, t - j\,\Delta t) \tag{5.5}$$

$$\mathbf{U}(x, y, t) = \begin{cases} \mathbf{U}_{\text{initial}}(x, y), & 0 \leqslant t < \Delta t \\ 0, & t < 0. \end{cases} \tag{5.6}$$

Now by taking the Fourier–Laplace transforms of difference equations (5.4) and (5.5) it is straightforward to find after using initial conditions (5.6) that the equation for the transform of $\mathbf{U}$ denoted by $\tilde{\mathbf{U}}$ is

$$\tilde{\bar{\mathbf{A}}}\,\tilde{\mathbf{U}} = \tilde{\mathbf{G}}, \tag{5.7}$$

where $\tilde{\mathbf{G}} = i(\tilde{\mathbf{H}} + (\bar{\omega}/2\pi\omega)\,\tilde{\mathbf{U}}_{\text{initial}})$. Here an overbar is used to denote the variables and parameters associated with the finite difference equations. This is to distinguish them from those of the original partial differential equations. The coefficient matrix $\tilde{\bar{\mathbf{A}}}$ of (5.7) is the same as that of Eq. (3.4), provided the transform variables α, β, and ω in (3.4a) are replaced by $\bar{\alpha}$, $\bar{\beta}$, and $\bar{\omega}$, respectively. $\bar{\alpha}$, $\bar{\beta}$, and $\bar{\omega}$ are the effective wave numbers and frequency of the difference scheme given by (2.5) and (4.6). It will be shown below that it is possible to choose Δt so that the finite difference marching scheme of (5.1) and (5.2) will always operate in the range of $\omega\,\Delta t$ for which $\bar{\omega} \simeq \omega$ as discussed at the end of Section 4. Also if only disturbances with wave lengths longer than or equal to $5\,\Delta x$ or $5\,\Delta y$, whichever is the larger, are considered, the wave numbers of the finite difference scheme are equal to those of the Fourier transforms, i.e., $\bar{\alpha} \simeq \alpha$ and $\bar{\beta} \simeq \beta$. Thus (5.7), to the numerical accuracy considered, is identical to the transform of the Euler equations (3.4). The matrices $\mathbf{A}$ and $\bar{\mathbf{A}}$, being equal, would have the same eigenvalues and eigenvectors. In other words, other than the spurious numerical waves contained in them, finite difference equations (5.1) and (5.2) support the same entropy, vorticity, and acoustic waves as the linearized Euler equations (3.1). The dispersion relations of these waves are identical, guaranteeing that the computed wave speeds and other wave propagation characteristics including isotropy and nondispersiveness are the same as those of the original partial differential equations. For this reason the finite difference scheme (5.1)–(5.2) will be referred to as a DRP scheme.

To implement the DRP scheme of (5.1)–(5.2) the size of the time step Δt must be chosen small enough to avoid numerical instability. To establish a criterion for determining such a Δt consider the pressure field of the finite difference equations (5.4) and (5.5). It is given by the sum of the fourth components of the two acoustic wave vectors of the solution of (5.7) (see (3.9) for their counterparts for the linearized Euler equations). By inverting the Fourier–Laplace transforms it is easy to find

$$p(x, y, t) = \int_\Gamma \iint_{-\infty}^{\infty} \frac{i[\rho_0 a_0^2 \bar{\alpha}\tilde{\mathbf{G}}_2 + \bar{\beta}\tilde{\mathbf{G}}_3 + (\bar{\omega} - \bar{\alpha}u_0)\,\tilde{\mathbf{G}}_4]}{(\bar{\omega} - \bar{\alpha}u_0)^2 - a_0^2(\bar{\alpha}^2 + \bar{\beta}^2)} \times e^{i(\alpha x + \beta y - \omega t)}\,d\alpha\,d\beta\,d\omega, \tag{5.8}$$

where $\bar{\alpha}(\alpha)$, $\bar{\beta}(\beta)$, and $\bar{\omega}(\omega)$ and its inverse $\omega = \omega(\bar{\omega})$ are given by (2.5) and (4.6). From the theory of Laplace transform it is well known that for large t the dominant contribution to the ω-integral comes from the residue of the pole of the integrand which has the largest imaginary part in the complex ω-plane. In (5.8) the pole corresponding to the outgoing acoustic wave is given implicitly by

$$\bar{\omega}(\omega) = \bar{\alpha}(\alpha)\,u_0 + a_0(\bar{\alpha}^2(\alpha) + \bar{\beta}^2(\beta))^{1/2}. \tag{5.9}$$

As has been discussed in Section 4 for a given $\bar{\omega}$ there are four values of ω. Thus there are four wave solutions associated with the $\bar{\omega}$ pole of (5.9), three of which are spurious. Let the roots be denoted by ω_k $(k = 1, 2, 3, 4)$ with ω_1 corresponding to the physical acoustic wave. On completing the contour in the lower half ω-plane by a large

semi-circle, by the residue theorem, the pressure field given by (5.8) becomes

$$p(x,y,t)=\sum_{k=1}^{4} -(2\pi i) \times\left[\int\int_{-\infty}^{\infty} \frac{i[\rho_0 a_0^2\bar{\alpha}\tilde{\mathbf{G}}_2+\bar{\beta}\tilde{\mathbf{G}}_3+(\bar{\omega}-u_0\bar{\alpha})\,\tilde{\mathbf{G}}_4]}{2(\bar{\omega}-\bar{\alpha}u_0)^{(\partial\bar{\omega}/\partial\omega)}}\Bigg|_{\omega=\omega_k} \times e^{i(\alpha x+\beta y)}\,d\alpha\,d\beta\right] e^{-i\omega_k t}. \tag{5.10}$$

To obtain numerical stability a sufficient condition is

$$\mathrm{Im}(\omega_k)\leqslant 0, \qquad k=1,2,3,4. \tag{5.11}$$

It is to be noted from Fig. 1 that for arbitrary values of α and β the inequalities

$$\bar{\alpha}\,\Delta x<1.75, \qquad \bar{\beta}\,\Delta y<1.75 \tag{5.12}$$

hold true. Substitution of (5.12) into (5.9) and upon multiplying by Δt it is found that

$$\bar{\omega}\,\Delta t\leqslant\frac{1.75a_0}{\Delta x}\left[M+\left(1+\left(\frac{\Delta x}{\Delta y}\right)^2\right)^{1/2}\right]\Delta t, \tag{5.13}$$

where $M=u_0/a_0$ is the mean flow Mach number. From Fig. 3 it is clear that if $|\bar{\omega}\,\Delta t|$ is less than 0.4 then all the roots of ω_k, especially the spurious roots, are damped. Therefore to ensure numerical stability it is sufficient by (5.13) to restrict Δt to less than $\Delta t_{\max}$ where $\Delta t_{\max}$ is given by

$$\Delta t_{\max}=\frac{0.4}{1.75[M+(1+(\Delta x/\Delta y)^2)^{1/2}]}\frac{\Delta x}{a_0}. \tag{5.14}$$

Similar analysis for the entropy and the vorticity wave modes of the finite difference scheme yields the criterion for numerical stability

$$\Delta t<\frac{0.4}{1.75M}\frac{\Delta x}{a_0}; \tag{5.15}$$

(5.14) is a more stringent condition than (5.15). Therefore, for $\Delta t<\Delta t_{\max}$ the DRP scheme would be numerically stable.

6. NUMERICAL DAMPING

The time discretization scheme discussed in Section 4 not only introduces spurious numerical solutions but also numerical damping of the physical waves in the computation. For accurate acoustic prediction numerical damping is most undesirable. It turns out that the amount of damping depends on the size of the time step, Δt, used. Here a discussion of how to control the effect of numerical damping by the proper selection of Δt is provided.

It can be seen in Fig. 3b that within the numerically stable range of the DRP scheme ($\bar{\omega}\,\Delta t<0.4$) the physical wave solution (the one with $\bar{\omega}\simeq\omega$) has a small imaginary part. By (5.10) this will lead to a time damping factor of the form $\exp(\omega_i t)$, where t is the lapsed time and ω_i is the imaginary part of ω_1 (the root which yields the physical solution). The value of $\omega_i\,\Delta t$ given by the finite difference scheme is a strong function of $\bar{\omega}\,\Delta t$. This relationship may be represented by the equation

$$-\omega_i\,\Delta t=Q(\bar{\omega}\,\Delta t). \tag{6.1}$$

Figure 4 shows a typical graph of the function $Q(\bar{\omega}\,\Delta t)$ for the case $\sigma=0.36$. The prominent feature of this graph is the steep gradient implying a large change in $\omega_i\,\Delta t$ for a relatively small change in $\bar{\omega}\,\Delta t$.

Suppose the distance between the acoustic sources and the computational boundary is $N\,\Delta x$, where N is the number of mesh spacings. The time needed for acoustic waves to propagate to the edge of the computation domain against a mean flow u_0 is $N\,\Delta x/(a_0-u_0)$. The total damping introduced by the finite difference scheme during this period of time is, therefore, equal to

$$\exp\left[\frac{\omega_i N\,\Delta x}{(1-M)\,a_0}\right],$$

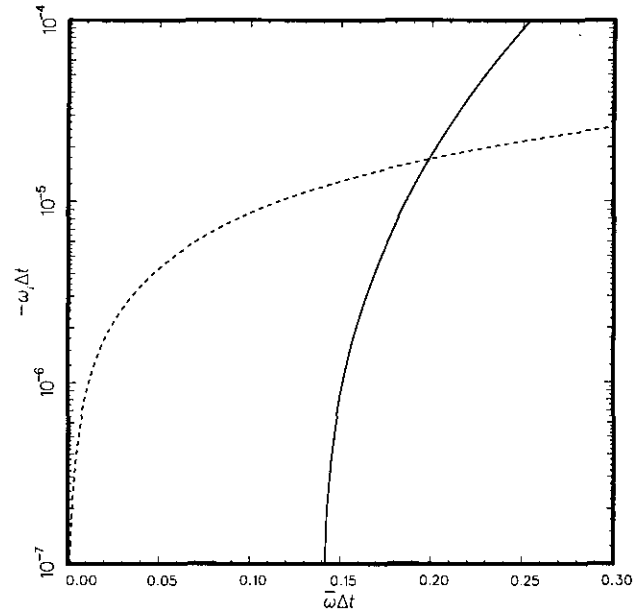

FIG. 4. Numerical damping as a function of frequency —— Eq. (6.1) with $\sigma=0.36$; – – – Eq. (6.5) with $\Delta x=\Delta y$, $M=0.5$, $N=100$, and $\Delta=0.5$.

where $M = u_0/a_0$ is the flow Mach number. Assume that a degradation of Δ dB (Δ may be 0.5, 1, or more, depending on the problem) of the computed acoustic wave solution due to numerical damping is acceptable. Then the maximum value of ω_i allowed is given by the equation

$$\exp\left[\frac{\omega_i N}{(1-M)}\frac{\Delta x}{a_0}\right] = 10^{-\Delta/20}. \tag{6.2}$$

The natural logarithm of (6.2) yields

$$\frac{\omega_i N}{(1-M)}\frac{\Delta x}{a_0} = -\frac{\Delta}{20}\ln(10). \tag{6.3}$$

Since the amount of damping depends strongly on the frequency of the wave, to preserve the quality of the computed acoustic waves it is sufficient that (6.3) is true for the highest frequency encountered in the finite difference computation. The highest computed frequency of the DRP scheme is given by Eq. (5.13), i.e.,

$$\bar{\omega}\,\Delta t = 1.75\left[M + \left(1 + \left(\frac{\Delta x}{\Delta y}\right)^2\right)^{1/2}\right]\frac{a_0\,\Delta t}{\Delta x}. \tag{6.4}$$

By eliminating $\Delta x/a_0$ from (6.3) and (6.4) it is easy to find

$$\bar{\omega}\,\Delta t = 1.75\left[M + \left(1 + \left(\frac{\Delta x}{\Delta y}\right)^2\right)^{1/2}\right] \times \frac{20}{\Delta \ln(10)}\frac{N}{1-M}(-\omega_i\,\Delta t). \tag{6.5}$$

The two equations (6.1) and (6.2) may be solved simultaneously for $\bar{\omega}\,\Delta t$ and $(-\omega_i\,\Delta t)$, the highest frequency and damping rate of the DRP scheme. This can easily be done graphically by finding the intersection of the two graphs as illustrated in Fig. 4. In this figure the numerical values of the various parameters are taken to be

$$\Delta x = \Delta y, \quad M = 0.5, \quad N = 100, \quad \Delta = 0.5.$$

Let the value of $\bar{\omega}\,\Delta t$ found in this way be Ω ($\Omega \simeq 0.19$ in Fig. 4). Then on eliminating $\bar{\omega}\,\Delta t$ in (6.4) the size of the time step Δt sufficient to meet the numerical damping criterion is given by

$$\Delta t = \frac{\Omega}{1.75[M + (1 + (\Delta x/\Delta y)^2)^{1/2}]}\frac{\Delta x}{a_0}. \tag{6.6}$$

In the numerical simulations to be discussed later in Section 8 it is found that (6.6) is a more stringent criterion than that required for numerical stability (Eq. (5.14)). In other words to avoid excessive numerical damping a small time step is needed.

7. RADIATION AND OUTFLOW BOUNDARY CONDITIONS

Many interesting acoustic problems are exterior problems. To simulate this class of problems it is necessary to impose radiation and outflow boundary conditions at the edges of the finite computation domain. To ensure that the computed solutions are of high quality these boundary conditions must be sufficiently transparent to the outgoing disturbances so that they exit the computation domain without significant reflections. As discussed in Section 3 the linearized Euler equations can support three types of waves. Thus, in general, the outgoing disturbances would contain a combination of acoustic, entropy, and vorticity waves, each having distinct wave propagation characteristics. In this section a set of radiation and outflow boundary conditions compatible with the DRP scheme will be developed. The effectiveness of these boundary conditions will be tested in the next section.

Consider the exterior problem involving a uniform flow of velocity u_0 and sound speed a_0 past some arbitrary acoustic, vorticity, and entropy sources as shown in Fig. 5. It will be assumed that the boundaries of the computation domain are quite far from the sources. From the analysis of Section 3 it is clear that at the outflow boundary on the right of Fig. 5 the outgoing disturbances would, in general, contain a superposition of acoustic, entropy, and vorticity waves. On the other hand, at the top and bottom boundaries, as well as the left inflow boundary of the computation domain, the outgoing disturbances consist of only acoustic waves. Now that the boundaries are far from the sources, the outgoing waves in the regions close to boundaries are, therefore, given by the asymptotic solutions of the DRP

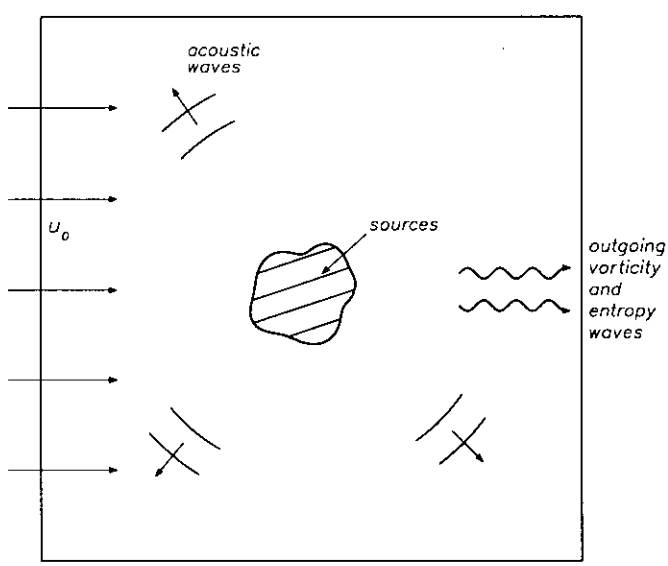

FIG. 5. Acoustic, vorticity, and entropy wave sources in a uniform flow.

scheme (5.1) and (5.2) or the more general finite difference equations (5.4) and (5.5). The importance of using the asymptotic solutions of the finite difference equations to develop radiation boundary conditions has recently been pointed out by the present authors [21]. However, in the useful range of the wave numbers the DRP scheme and the partial differential equations have (almost) identical dispersion relations so that they have the same asymptotic solutions. These solutions are given by (3.14), (3.16), and (3.18). A set of radiation and outflow boundary conditions will now be constructed from these asymptotic solutions.

7.1. *Radiation Boundary Conditions*

At boundaries where there are only outgoing acoustic waves the solution is given by (3.18) which may be rewritten in the form

$$\begin{bmatrix} \rho \\ u \\ v \\ p \end{bmatrix} \equiv \begin{bmatrix} \rho_a \\ u_a \\ v_a \\ p_a \end{bmatrix} = \frac{F(r/V(\theta)-t,\theta)}{r^{1/2}} \begin{bmatrix} \dfrac{1}{a_0^2} \\ \dfrac{\hat{u}(\theta)}{\rho_0 a_0} \\ \dfrac{\hat{v}(\theta)}{\rho_0 a_0} \\ 1 \end{bmatrix} + O(r^{-3/2}), \tag{7.1}$$

where $V(\theta) = a_0[M\cos\theta + (1-M^2\sin^2\theta)^{1/2}]$. The subscript "$a$" in (ρ_a, u_a, v_a, p_a) above indicates that the disturbances are associated with the acoustic waves alone. By taking the time (t) and r derivatives of (7.1) it is straightforward to find that for arbitrary function F the acoustic disturbances satisfy the equations

$$\left(\frac{1}{V(\theta)}\frac{\partial}{\partial t} + \frac{\partial}{\partial r} + \frac{1}{2r}\right)\begin{bmatrix} \rho \\ u \\ v \\ p \end{bmatrix} = 0 + O(r^{-5/2}); \tag{7.2}$$

(7.2) is the sought after radiation boundary condition.

7.2. *Outflow Boundary Conditions*

At the outflow region the outgoing disturbances, in general, consist of a combination of acoustic, entropy, and vorticity waves. Thus by means of the asymptotic solutions of (3.14), (3.16), and (3.18) the density, velocity, and pressure fluctuations are given by

$$\begin{bmatrix} \rho \\ u \\ v \\ p \end{bmatrix} = \begin{bmatrix} \chi(x-u_0t, y) + \rho_a \\ \dfrac{\partial\psi}{\partial y}(x-u_0t, y) + u_a \\ -\dfrac{\partial\psi}{\partial x}(x-u_0t, y) + v_a \\ p_a \end{bmatrix} + \cdots, \tag{7.3}$$

where the explicit form of (ρ_a, u_a, v_a, p_a) may be found in (7.1). The functions χ, ψ, and F are entirely arbitrary. It is observed that the total pressure fluctuation comes only from the acoustic component of the outgoing disturbances. Thus the appropriate outflow boundary condition for p is the same as that of (7.2). On writing out in Cartesian coordinates it is

$$\frac{1}{V(\theta)}\frac{\partial p}{\partial t} + \cos\theta\frac{\partial p}{\partial x} + \sin\theta\frac{\partial p}{\partial y} + \frac{p}{2r} = 0, \tag{7.4}$$

where θ is the angular coordinate of the boundary point.

By differentiating the expression for ρ in (7.3) with respect to t and x the following equation is found:

$$\frac{\partial\rho}{\partial t} + u_0\frac{\partial\rho}{\partial x} = \frac{\partial\rho_a}{\partial t} + u_0\frac{\partial\rho_a}{\partial x}. \tag{7.5}$$

But $\rho_a = p_a/a_0^2 = p/a_0^2$ and p is known from (7.4). By eliminating ρ_a the outflow boundary condition for ρ becomes

$$\frac{\partial\rho}{\partial t} + u_0\frac{\partial\rho}{\partial x} = \frac{1}{a_0^2}\left(\frac{\partial p}{\partial t} + u_0\frac{\partial p}{\partial x}\right). \tag{7.6}$$

Similarly by differentiating the expressions of u and v in (7.3) it is easy to find

$$\frac{\partial u}{\partial t} + u_0\frac{\partial u}{\partial x} = \frac{\partial u_a}{\partial t} + u_0\frac{\partial u_a}{\partial x} \tag{7.7}$$

$$\frac{\partial v}{\partial t} + u_0\frac{\partial v}{\partial x} = \frac{\partial v_a}{\partial t} + u_0\frac{\partial v_a}{\partial x}. \tag{7.8}$$

However, the acoustic component satisfies the momentum equations of the (linearized) Euler equations, i.e.,

$$\frac{\partial u_a}{\partial t} + u_0\frac{\partial u_a}{\partial x} = -\frac{1}{\rho_0}\frac{\partial p_a}{\partial x} = -\frac{1}{\rho_0}\frac{\partial p}{\partial x} \tag{7.9}$$

$$\frac{\partial v_a}{\partial t} + u_0\frac{\partial v_a}{\partial x} = -\frac{1}{\rho_0}\frac{\partial p_a}{\partial y} = -\frac{1}{\rho_0}\frac{\partial p}{\partial y}. \tag{7.10}$$

Upon eliminating u_a and v_a from (7.7) and (7.8) by (7.9) and (7.10) the outflow boundary conditions for the velocity components may be written as

$$\frac{\partial u}{\partial t} + u_0\frac{\partial u}{\partial x} = -\frac{1}{\rho_0}\frac{\partial p}{\partial x} \tag{7.11}$$

$$\frac{\partial v}{\partial t} + u_0\frac{\partial v}{\partial x} = -\frac{1}{\rho_0}\frac{\partial p}{\partial y}. \tag{7.12}$$

In summary, the outflow boundary conditions are

$$\begin{aligned}
&\frac{\partial \rho}{\partial t}+u_0\frac{\partial \rho}{\partial x}=\frac{1}{a_0^2}\left(\frac{\partial p}{\partial t}+u_0\frac{\partial p}{\partial x}\right)\\
&\frac{\partial u}{\partial t}+u_0\frac{\partial u}{\partial x}=-\frac{1}{\rho_0}\frac{\partial p}{\partial x}\\
&\frac{\partial v}{\partial t}+u_0\frac{\partial v}{\partial x}=-\frac{1}{\rho_0}\frac{\partial p}{\partial y}\\
&\frac{1}{V(\theta)}\frac{\partial p}{\partial t}+\cos\theta\frac{\partial p}{\partial x}+\sin\theta\frac{\partial p}{\partial y}+\frac{p}{2r}=0.
\end{aligned} \tag{7.13}$$

7.3. *Implementation of Radiation and Outflow boundary Conditions*

The central difference scheme for approximating spatial derivatives introduced in Section 2 invariably gives rise to ghost points at the boundary of the computation domain. For a seven-point stencil three ghost points are created. To advance the entire computation to the next time level, a way to calculate the unknowns at the ghost points must be specified. Here it is suggested that this is done using the radiation or outflow boundary conditions.

Figure 6 shows the upper right-hand corner of the computation domain. Three columns or rows of ghost points are added to form a boundary region surrounding the original computation domain. For grid points inside and on the boundary of the interior region the DRP scheme of (5.1) and (5.2) is used to advance the calculation of the unknowns to the next time level. In the boundary region it will be assumed that the solution is made up of outgoing disturbances satisfying the radiation or outflow boundary conditions of (7.2) or (7.13). The time derivatives of these equations are discretized in the same manner as described in Section 4. With the same time marching scheme all the unknowns in the boundary as well as the interior regions can be advanced simultaneously. To approximate spatial derivatives symmetric spatial stencils are not always possible for the points in this region. Optimized backward differences (involving seven points) are to be used whenever necessary. An example of such a backward difference stencil is illustrated by that of the corner point "*B*" in Fig. 6. In the boundary region the domain of dependence of the outgoing waves is consistent with that of the backward difference approximations. Unlike the use of unsymmetric stencil at interior points, where waves may propagate in any direction, no numerical instability would be created unless there are strong reflections of waves back into the interior.

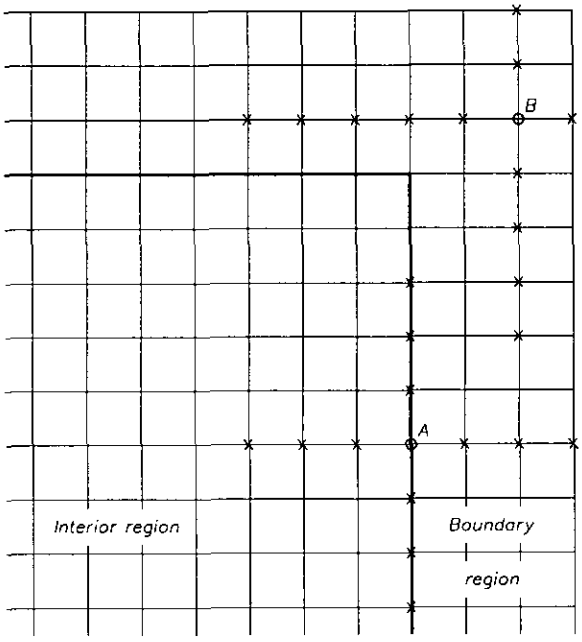

FIG. 6. The interior and boundary regions of the computation domain. Also shown are typical stencils for interior points (A) and boundary or ghost points (B).

8. DIRECT NUMERICAL SIMULATIONS

To test the effectiveness of the DRP schemes and independently the radiation and outflow boundary conditions of Section 7, a sequence of direct numerical simulations has been carried out. As a part of this effort three exact solutions of the linearized Euler equations have also been developed. These solutions are reported in Appendix B. The first solution involves an initial axisymmetric pressure pulse. When released at time $t=0$ an acoustic pulse is generated. The wave front of the acoustic pulse expands radially. But because of the mean flow the whole wave pattern is being convected downstream at the same time. The other two solutions involve initial distributions of vorticity and density inhomogeneties. These vorticity and density pulses are convected downstream by the mean flow without any distortion. These exact solutions will be used to compare with the numerical solutions. They provide a standard for measuring the accuracy and quality of the computed solutions.

Due to space limitation only the results of one special simulation involving all three types of disturbances will be described in detail here. Some general results observed in other simulations will, however, be briefly discussed. In the special simulation an acoustic pulse is generated by an initial Gaussian pressure distribution at the center of the computation domain. The mean flow Mach number is taken to be 0.5. Downstream of the pressure pulse at a distance equal to $\frac{1}{3}$ of the length of the computation domain a vorticity pulse and an entropy pulse (also with Gaussian distribution) are generated at the same time. Since the acoustic pulse travels three times faster than the vorticity and entropy pulses in the downstream direction, this arrange-

ment ensures that all the three pulses reach the outflow boundary simultaneously. In this way it is possible to obtain a critical test of the effectiveness of the radiation as well as the outflow boundary conditions in a single simulation.

In the simulation the variables are nondimensionalized by the following scales:

$$\text{length scale} = \Delta x = \Delta y$$
$$\text{velocity scale} = a_0$$
$$\text{time scale} = \Delta x/a_0$$
$$\text{density scale} = \rho_0$$
$$\text{pressure scale} = \rho_0 a_0^2.$$

The computation domain is divided into a 200×200 mesh. The parameters of the initial pressure, vorticity, and entropy pulses are (see Appendix B):

$$\text{pressure pulse amplitude } \varepsilon_1 = 0.01,$$
$$\text{half-width} = 3.0$$
$$\text{entropy pulse amplitude } \varepsilon_2 = 0.001,$$
$$\text{half-width} = 5.0$$
$$\text{vorticity pulse amplitude } \varepsilon_3 = 0.0004,$$
$$\text{half-width} = 5.0.$$

The computer code in this work is written for the full Euler equations. However, the disturbance amplitudes have been chosen to be relatively small so that the numerical solutions may be compared with the exact solution of the linearized equations.

The results of the special simulation will now be presented. Figure 7a shows the density contours of the acoustic pulse at the center of the computation domain and the entropy pulse downstream at time $t = 0$. The vorticity pulse has no density fluctuations and therefore, cannot be seen in this figure. Figure 7b shows the computed density contours after 500 time steps ($\Delta t = 0.0569$). At this time the radius of the acoustic pulse has expanded considerably while that of the entropy pulse remains the same. The centers of the two pulses have moved downstream by an equal distance. Figure 7c shows the locations of the two pulses at 1000 time steps. The acoustic pulse has now caught up with the entropy pulse. At a slightly later time the density contours of the pulses merge and exit the outflow boundary together. Based on the 1% contour plot no noticeable reflections have been observed, indicating that the outflow boundary condition is transparent. At a still later time the acoustic pulse reaches and leaves the computation domain through the top and bottom boundaries. Again little or no reflections can be found (to 1% of the incident wave amplitude). This is shown in Figure 7d. Finally at 3200 time steps the acoustic wave front reaches the inflow boundary on the left. The pulse exits the computation domain again with little observable reflections.

Figure 8a shows the pressure contours of the acoustic pulse at 500 time steps in the simulation. Since both the entropy pulse and the vorticity pulse contain no pressure fluctuations they are not seen in this figure. Figure 8b gives the pressure contours at 1250 time steps. At this time, part of the acoustic pulse has already left the outflow boundary. Once more no noticeable reflections can be detected. As the simulations goes on, the pressure contours leave the top and bottom boundaries and then the left boundary. The radiation boundary conditions imposed in these regions appear to be very effective. Little reflections are observed.

Figure 9a shows the contours of the magnitude of the velocity fluctuations (or speed) at 500 time steps. The center circles are those of the acoustic pulse. The circles to the right are contours associated with the vorticity pulse. The contours are constructed by interpolation between mesh points. To the accuracy allowed by this procedure the expanding circles are, indeed, circular so that the computed acoustic wave speed is the same in all directions. Figure 9b gives the speed contours at 1500 time steps. At this time the main part of the acoustic pulse has already left the outflow boundary. The vorticity pulse, having a slower velocity, has, however, not completely left the right boundary. A small piece of it can still be seen just at the outflow boundary. In this figure the 1% contour exhibits some minor wiggles. A closer examination of the computed data indicates that they are generated by the graphic program and not by the simulation.

The computed density waveform along the x-axis at 500 time steps is given in Fig. 10a. Shown by the dotted line is the exact solution. The exact and computed waveforms are clearly almost identical. Figure 10b provides both the computed and the exact waveforms at 1000 time steps when the acoustic pulse has caught up with the entropy pulse. Again there is good agreement between the two waveforms. Figures 11a and 11b provide comparisons between the computed and the exact pressure waveforms at 500 and 1150 time steps. It is evident that the agreements are good. Extensive comparisons between the computed density, pressure, and velocity waveforms have been carried out at different directions of propagation up to 4500 time steps when nearly all the disturbances have exited the computation domain. Good agreements are found regardless of the direction of wave propagation. Such good agreements are maintained in time up to the termination of the simulation.

In addition to the simulation described in detail above, several series of simulations using more than one acoustic pulse generated at various locations of the computation

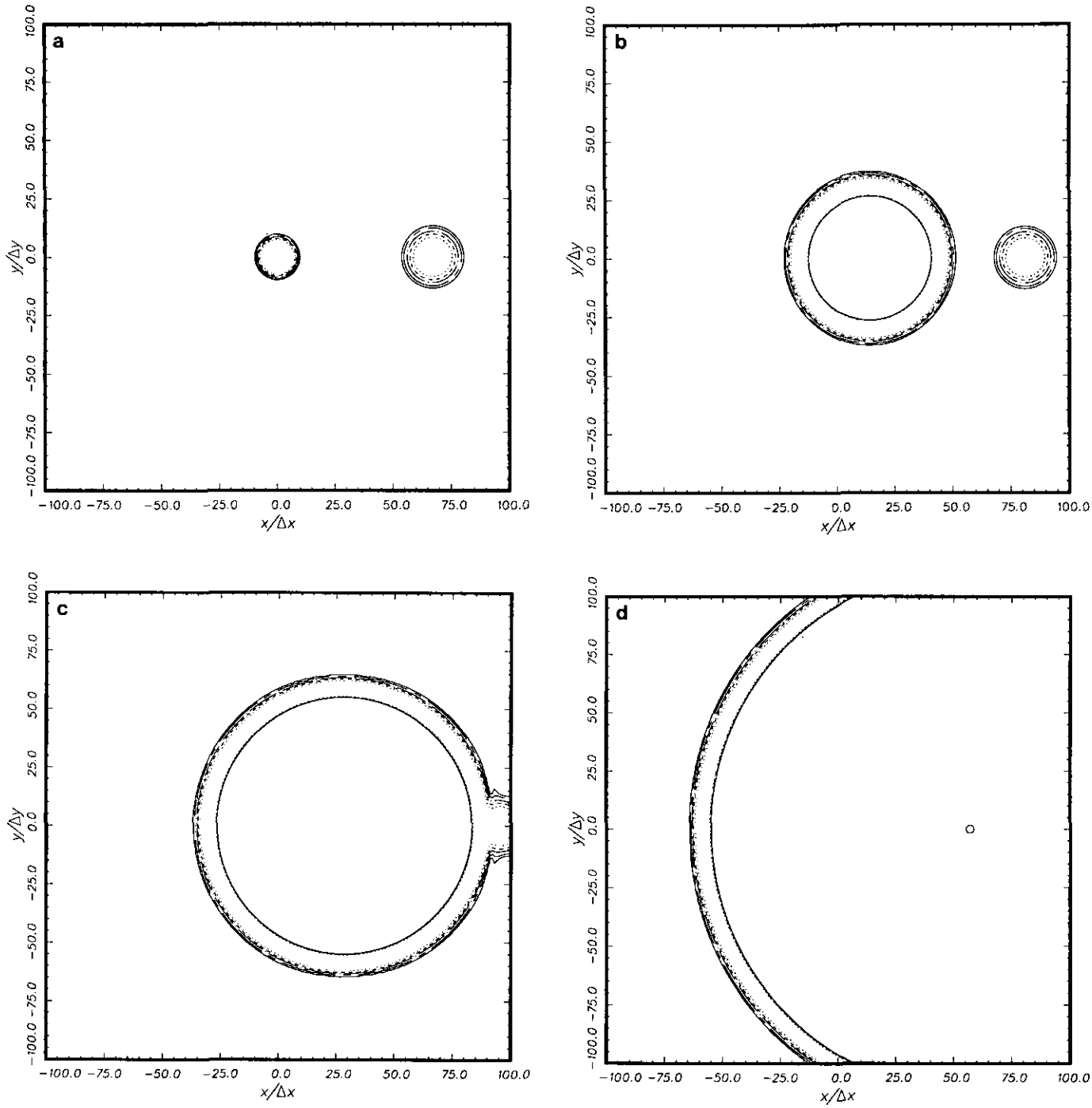

FIG. 7. Density contours. $M = 0.5$. Intensity relative to peak acoustic disturbance density at the outflow boundary: ····· 0.2; — — 0.1; —·— 0.05; — – 0.02; ——— 0.01. (a) zero time steps; (b) 500 time steps; (c) 1000 time steps; (d) 2000 time steps.

domain have been carried out. Good agreements are again found when compared with the exact solutions of the linearized Euler equations. This is true as long as the predominant part of the wave spectrum has wave numbers α and β such that $\alpha\,\Delta x$ and $\beta\,\Delta y$ are both less than 1.4. Overall, the results of all the simulations strongly suggest that the DRP scheme can be relied on to yield accurate results when used to simulate isotropic, nondispersive, and nondissipative acoustic, vorticity, and entropy waves. Furthermore, the scheme can be expected to reproduce the wave speeds correctly.

It is important to point out that the radiation boundary

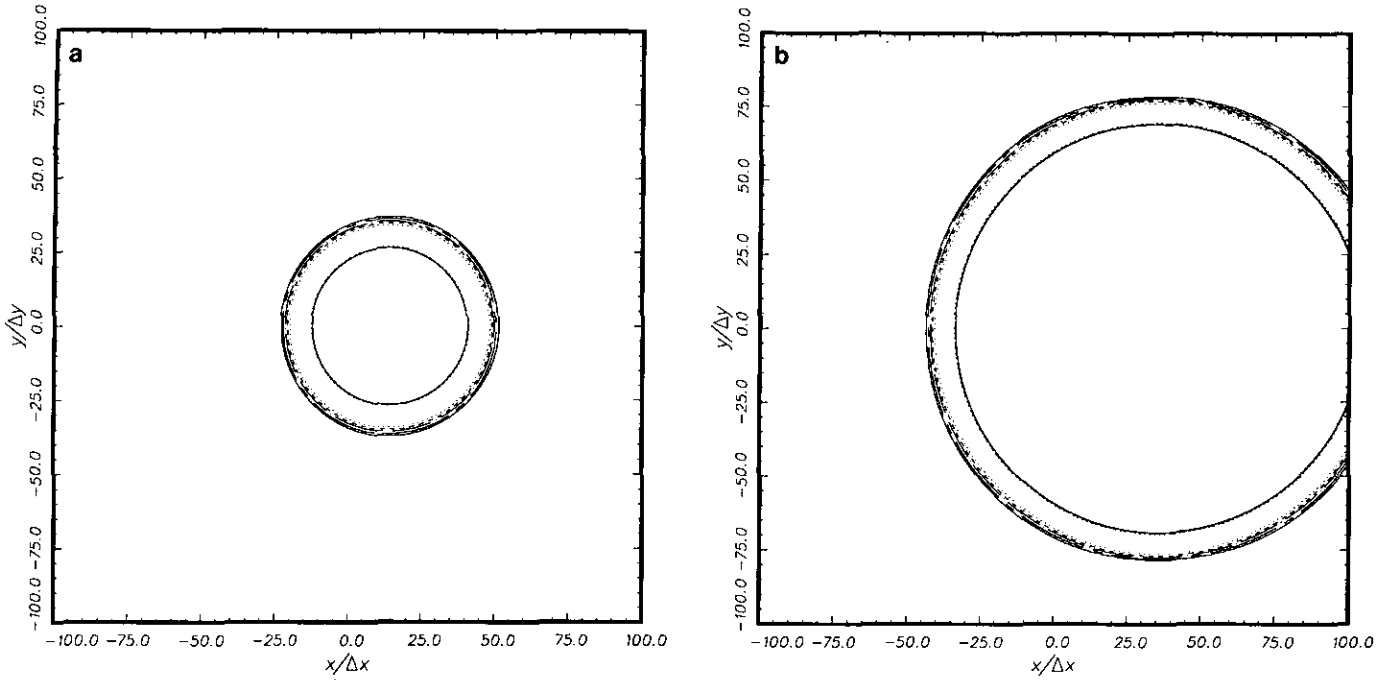

FIG. 8. Pressure contours. $M = 0.5$. Intensity relative to peak disturbance pressure at the outflow boundary: ····· 0.2; – – – 0.1; —·— 0.05; — — 0.02; ——— 0.01. (a) 500 time steps; (b) 1250 time steps.

conditions (7.2) and the outflow boundary conditions (7.13) depend on the angle θ. If the boundaries are far from the source then the exact location of the source is not important. But if the source is close to a boundary the effectiveness of these boundary conditions would deteriorate as the direction of wave propagation is in error. An extensive series of tests involving an acoustic source put closer and closer to the boundaries have been carried out. The radiation boundary conditions appear to perform quite well even when the center of the acoustic pulse is at 20 mesh points away from

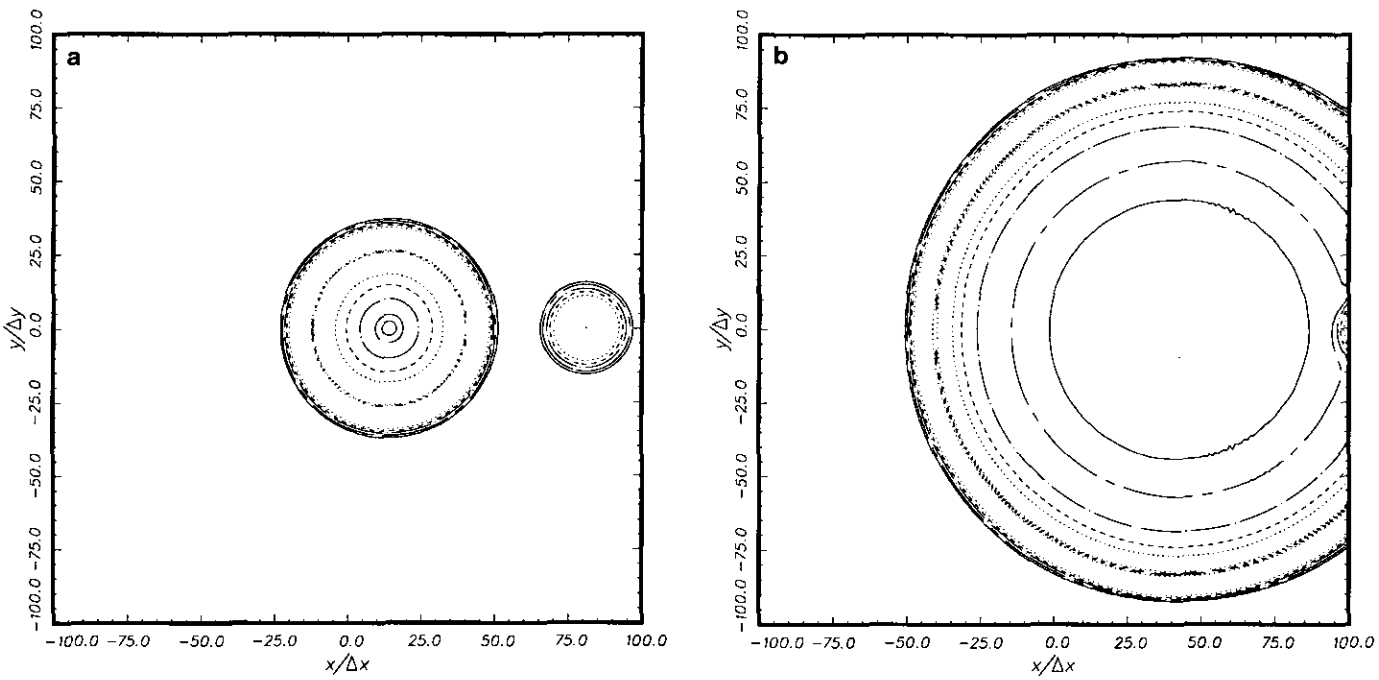

FIG. 9. Speed contours. $M = 0.5$. Intensity relative to peak disturbance speed at the outflow boundary: ····· 0.2; – – – 0.1; —·— 0.05; — — 0.02; ——— 0.01. (a) 500 time steps; (b) 1500 time steps.

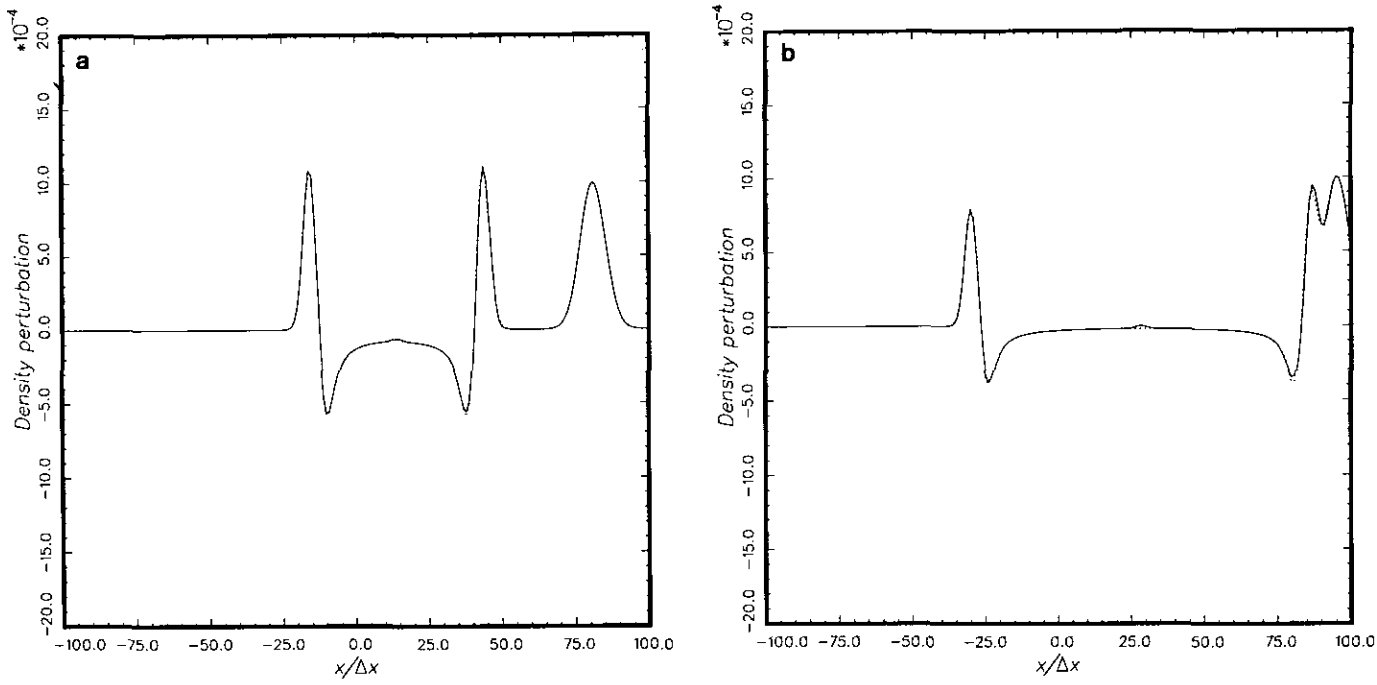

FIG. 10. Density waveform along the x-axis. $M = 0.5$: ····· exact solution; ——— computed solution. (a) 500 time steps; (b) 1000 time steps.

the boundary. The reflected wave amplitude is generally less than 2% of the incident wave amplitude. The outflow boundary conditions, on the other hand, have been observed to cause a moderate level of reflection; 15% for acoustic pulse initiated at 20 mesh points away. This is true with or without mean flow. Recall that the radiation and outflow boundary conditions were developed from asymptotic solutions; the degradation of the effectiveness of the boundary conditions for sources located close to a boundary should, therefore, be expected.

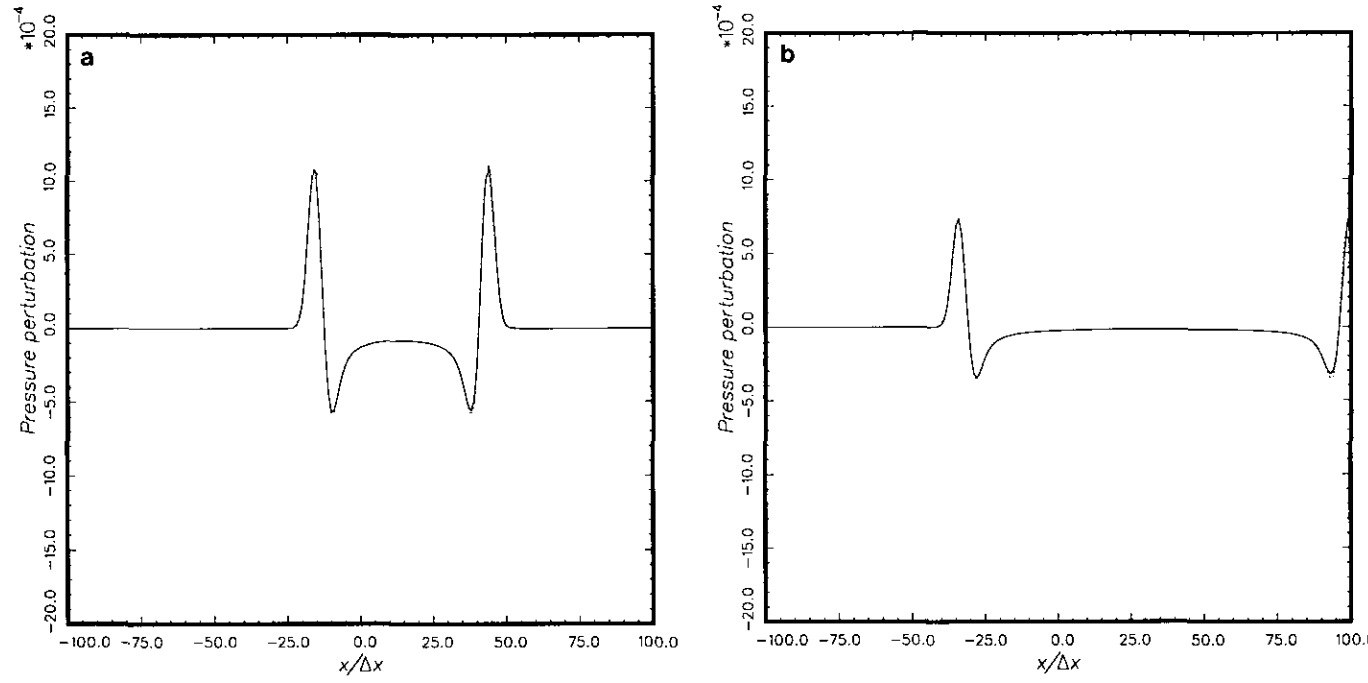

FIG. 11. Pressure waveform along the x-axis. $M = 0.5$: ····· exact solution; ——— computed solution. (a) 500 time steps; (b) 1150 time steps.

9. DISCUSSION

The central idea of this paper is that a time marching high order finite difference scheme can faithfully reproduce the three types of waves, namely the acoustic, vorticity, and entropy waves, of the linearized Euler equations if the dispersion relations of the finite difference scheme are the same as those of the partial differential equations. A way to construct such a DRP scheme is proposed. The major restriction appears to be that the dispersion relations can be preserved only for waves with wave lengths longer than four or five mesh spacings.

In the past, the importance of the dispersion relations of finite difference schemes has been recognized by a number of investigators, e.g., Vichnevetsky and coworkers [22, 23] and Trefethen [24]. Through the use of the dispersion relation these authors were able to predict the group and phase velocities of the computed wave solutions. In developing the dispersion relation of a finite difference equation they followed the elementary plane wave method commonly used in wave propagation theory [10]. This way of obtaining the dispersion relation is simple and convenient. In this paper the method of Fourier–Laplace transforms is used instead. Although it is slightly more complicated, the transform method, however, offers a number of significant advantages. Most important of all, it provides a way to investigate possible numerical instabilities inherent in the finite difference scheme. In addition the transform method can be used to construct asymptotic solutions of the finite difference equations. This possibility has recently been exploited by the present authors in investigating the effect of numerical dispersion on finite difference solutions of propeller noise problems [25] and in constructing nonreflective boundary conditions for the Helmholtz equation [21]. Here the asymptotic solutions are used to develop radiation and outflow boundary conditions for the DRP scheme. The effectiveness of these radiation and outflow boundary conditions has been confirmed by direct numerical simulations.

Traditional finite difference schemes for approximating the derivative of a function are often constructed by the truncated Taylor series method. In this work this standard method is not used. Instead the finite difference scheme is constructed by optimizing the approximation in the wave number and frequency space. Lele [26] in his work on compact finite difference schemes gave very detailed comparisons of the accuracies of the compact schemes, the standard schemes, and modified versions of the optimized scheme in approximating the spatial derivatives in wave number space. He showed that a pentadiagonal compact scheme can give accurate approximation for values of $\alpha\,\Delta x$ as large as 2.5. This is very attractive. Unfortunately, the computation time needed to implement the compact scheme is of an order of magnitude more than the simple optimized scheme discussed and used in this investigation. Also the compact scheme, together with the Runge–Kutta time marching method employed by Lele, is not dispersion relation preserving. There is, therefore, no guarantee that the waves as computed by such an elaborate scheme would propagate with the correct wave speeds.

One point that should be emphasized is that wave propagation involves the interplay between space and time. To be able to compute a wave solution accurately it is not sufficient to have good approximation of the spatial derivatives alone or of the time derivatives alone. Both must be well approximated in a related way as dictated by the dispersion relations of the original partial differential equations. If this is not done correctly the wave modes may become numerically coupled. When this happens the numerical solutions are liable to yield misleading results.

Finally, in this paper, for simplicity, most of the analyses have been carried out in two dimensions. All the results are, however, extendable to three dimensions in a straightforward manner. In three dimensions there are two linearly independent vorticity waves so that the linearized Euler equations support a total of five wave modes. Efforts are currently underway to test the applicability of the present computation scheme to the fully nonlinear Euler equations. It is believed that with suitable modifications the DRP scheme can provide high quality nonlinear wave solutions.

APPENDIX A: ASYMPTOTIC SOLUTIONS

A1. *Entropy Waves*

The entropy wave solution is given by Eq. (3.13). As noted before the contour Γ lies in the upper half ω-plane above all poles and singularities of the integrand. Thus the value ω in the denominator of (3.13) has a positive imaginary part. For large $|x|$ the contribution to the α-integrand comes mainly from the poles of the integrand. In this case the pole is given by the zeros of the dispersion relation, i.e., $\alpha = \omega/u_0$. The pole lies in the upper half α-plane as shown in Fig. 12. Now the α-integral can be evaluated by adding a large semi-circle in the upper (lower) half α-plane for x greater (less) than zero. Upon using the residue theorem it is easy to find

$$\rho(x, y, t) \sim \begin{cases} \displaystyle\int_\Gamma \int_{-\infty}^{\infty} \frac{2\pi i C_1}{-u_0}\, e^{i(x/u_0 - t)\omega + i\beta y}\, d\beta\, d\omega, \\ \qquad x \to \infty \\ 0, \qquad x \to -\infty, \end{cases}$$

or in a more convenient form,

$$\rho(x, y, t) = \begin{cases} \chi(x - u_0 t, y), & x \to \infty \\ 0, & x \to -\infty, \end{cases} \tag{A1}$$

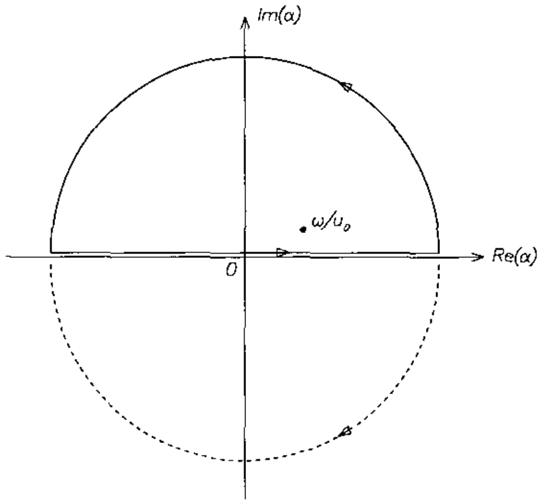

FIG. 12. Inversion contours and pole in the complex α-plane.

where the function χ depends on the initial conditions and the source distributions.

A2. *Vorticity Waves*

The vorticity wave solution can be found by inverting the Fourier–Laplace transforms of the second vector of (3.9). That is,

$$\mathbf{U}(x, y, t) = \int_\Gamma \iint_{-\infty}^{\infty} \frac{C_2}{\omega - \alpha u_0} \mathbf{X}_2 \times e^{i(\alpha x + \beta y - \omega t)}\, d\alpha\, d\beta\, d\omega. \tag{A2}$$

Since the first and last elements of $\mathbf{X}_2$ are zero, there is no density or pressure fluctuation associated with the vorticity waves. The poles of the above α-integral are the same as those of the entropy waves. The integral can, therefore, be evaluated in the same manner yielding

$$u(x, y, t) = \begin{cases} \dfrac{\partial \psi}{\partial y}, & x \to \infty \\ 0, & x \to -\infty \end{cases}$$
$$v(x, y, t) = \begin{cases} -\dfrac{\partial \psi}{\partial x}, & x \to \infty \\ 0, & x \to -\infty, \end{cases} \tag{A3}$$

where $\psi = \psi(x - u_0 t, y)$.

A3. *Acoustic Waves*

The acoustic wave solution can be obtained by inverting the Fourier–Laplace transforms of the last two vectors of (3.9). On writing out in full the formal solution becomes

$$\begin{bmatrix} \rho \\ p \end{bmatrix} = \int_\Gamma \iint_{-\infty}^{\infty} \frac{\rho_0 a_0^2(\alpha \tilde{G}_2 + \beta \tilde{G}_3) + (\omega - \alpha u_0)\tilde{G}_4}{(\omega - \alpha u_0)^2 - a_0^2(\alpha^2 + \beta^2)} \times \begin{bmatrix} \dfrac{1}{a_0^2} \\ 1 \end{bmatrix} e^{i(\alpha x + \beta y - \omega t)}\, d\alpha\, d\beta\, d\omega \tag{A4}$$

$$\begin{bmatrix} u \\ v \end{bmatrix} = \int_\Gamma \iint_{-\infty}^{\infty} \times \frac{(\omega - \alpha u_0)(\alpha \tilde{G}_2 + \beta \tilde{G}_3)/(\alpha^2 + \beta^2) + \tilde{G}_4/\rho_0}{(\omega - \alpha u_0)^2 - a_0^2(\alpha^2 + \beta^2)} \times \begin{bmatrix} \alpha \\ \beta \end{bmatrix} e^{i(\alpha x + \beta y - \omega t)}\, d\alpha\, d\beta\, d\omega \tag{A5}$$

Now the integrals of (A4) will be evaluated in the limit $(x^2 + y^2) \to \infty$. The β integral will be evaluated first. The poles in the β-plane are at $\beta_\pm$ which are given by

$$\beta_\pm = \pm i \left[\alpha^2 - \frac{(\omega - \alpha u_0)^2}{a_0^2} \right]^{1/2}. \tag{A6}$$

The branch cuts of the above square root function in the α-plane are taken to be

$$-\frac{\pi}{2} \leqslant \arg \left[\alpha^2 - \frac{(\omega - \alpha u_0)^2}{a_0^2} \right]^{1/2} \leqslant \frac{\pi}{2}, \tag{A7}$$

where the left (right) equality sign is to be used when ω is real and positive (negative). The branch cut configuration and the position of the inverse α-contour are shown in Fig. 13. This configuration is valid regardless of whether ω is real and positive or negative. In the β-plane the integrand of (A4) has a simple pole at β_+ in the upper half plane and

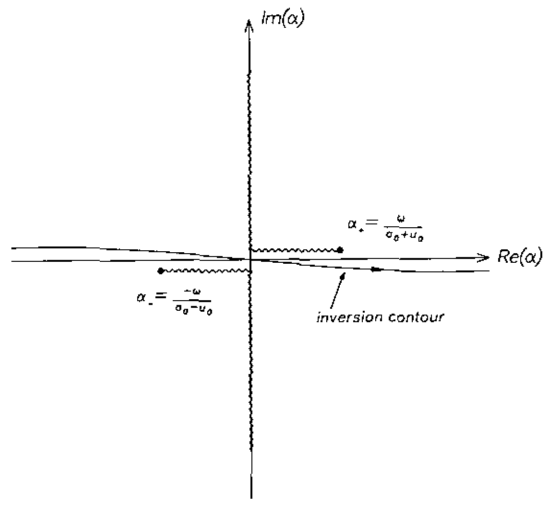

FIG. 13. The branch cut configuration and inversion contour in the complex α-plane.

a simple pole at β_- in the lower half plane (see Fig. 14). For $y>0$ ($y<0$) the inversion contour may be closed in the upper (lower) half plane by adding a large semi-circle as shown. By invoking the residue theorem, the expressions for ρ and p simplify to

$$\begin{bmatrix}\rho\\p\end{bmatrix}=\int_\Gamma\int_{-\infty}^{\infty}\frac{-\pi i}{a_0\beta_+}\,[\rho_0a_0^2(\alpha\tilde{G}_2+\beta_+\tilde{G}_3)+(\omega-\alpha u_0)\,\tilde{G}_4]\begin{bmatrix}\frac{1}{a_0^2}\\1\end{bmatrix}e^{i\Phi(\alpha,\theta)r-i\omega t}\,d\alpha\,d\omega. \tag{A8}$$

In (A8) r and θ are the polar coordinates and $\Phi=\alpha\cos\theta+i[\alpha^2-(\omega-\alpha u_0)^2/a_0^2]^{1/2}\sin\theta$.

In the far field, where $r\to\infty$, the α-integral of (A8) can be evaluated by the method of stationary phase. A straightforward application of this method gives

$$\begin{bmatrix}\rho\\p\end{bmatrix}\sim\int_{-\infty}^{\infty}\frac{-\pi i}{a_0\beta_s}\,[\rho_0a_0^2(\alpha_s\tilde{G}_2+\beta_s\tilde{G}_3)+(\omega-\alpha_s u_0)\tilde{G}_4]\begin{bmatrix}\frac{1}{a_0^2}\\1\end{bmatrix}\times\left(\frac{2\pi}{r\,|\Phi''|}\right)^{1/2}e^{i[r/V(\theta)-t]\omega+i\pi/4\,\mathrm{sgn}(\Phi'')}\,d\omega, \tag{A9}$$

where α_s is the stationary phase point, $\beta_s=\beta_+(\alpha_s)$, $\Phi''(\alpha_s)=\partial^2\Phi/\partial\alpha^2|_{\alpha=\alpha_s}$, and $V(\theta)=u_0\cos\theta+a_0(1-u_0^2\sin^2\theta/a_0^2)^{1/2}$. (A9) may be rewritten in the more convenient form

$$\begin{bmatrix}\rho\\p\end{bmatrix}=\frac{F(r/V(\theta)-t,\theta)}{r^{1/2}}\begin{bmatrix}\frac{1}{a_0^2}\\1\end{bmatrix}+O(r^{-3/2}). \tag{A10}$$

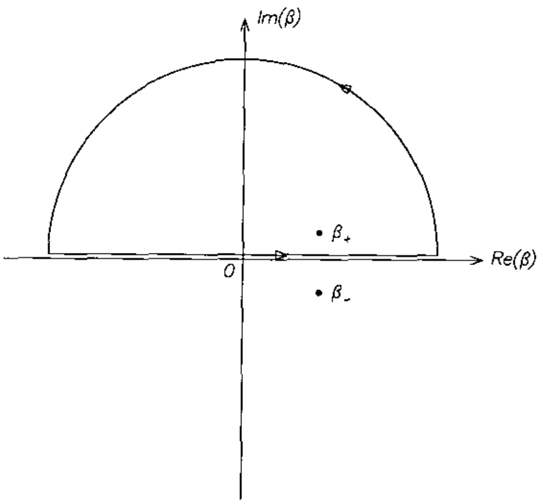

FIG. 14. The poles and inversion contour in the complex β-plane.

Finally, by evaluating the integrals of (A5) in exactly the same way, the asymptotic solution given by (3.18) can be easily derived.

APPENDIX B: EXACT SOLUTIONS OF THE LINEARIZED EULER EQUATIONS

Consider wave disturbances generated by initial excitations in a uniform mean flow of Mach number M. If the amplitude of the waves are small they are governed by the linearized Euler equations. To construct exact solutions of the linearized Euler equations it is advantageous to use a coordinate system moving with the mean flow. Let (x, y, t) and (x', y', t') be the Cartesian coordinates and time of the stationary and moving coordinate systems, respectively. It will be assumed that dimensionless variables (with respect to the scales given in Section 8) are used. The relationship between the two coordinate systems are

$$t'=t,\qquad x'=x-Mt,\qquad y'=y. \tag{B1}$$

In the moving frame of reference the linearized Euler equations may be written in the form

$$\frac{\partial}{\partial t'}\begin{bmatrix}\rho\\u\\v\\p\end{bmatrix}+\frac{\partial}{\partial x'}\begin{bmatrix}u\\p\\0\\u\end{bmatrix}+\frac{\partial}{\partial y'}\begin{bmatrix}v\\0\\p\\v\end{bmatrix}=0. \tag{B2}$$

B1. *Acoustic Waves*

Acoustic wave solutions can be found in terms of the velocity potential ϕ which is related to the physical variables by

$$\mathbf{v}=\nabla'\phi,\qquad p=-\frac{\partial\phi}{\partial t'},\qquad \rho=p. \tag{B3}$$

It is easy to find from (B2) and (B3) that the governing equation for ϕ is the simple wave equation. Consideration will now be restricted to cylindrical waves. For this family of waves the simple wave equation reduces to

$$\frac{\partial^2\phi}{\partial t'^2}-\left(\frac{\partial^2\phi}{\partial r'^2}+\frac{1}{r'}\frac{\partial\phi}{\partial r'}\right)=0, \tag{B4}$$

where r' is the radial distance in polar coordinates. Let the initial conditions be

$$t'=0,\qquad \phi=0,\qquad \frac{\partial\phi}{\partial t'}=-g(r'). \tag{B5}$$

In (B5) the function g is arbitrary. The initial value problem

of (B4) and (B5) can be solved by means of the order-zero Hankel transform. If $\tilde{g}(\xi)$ is the Hankel transform of the initial data it is straightforward to find that the velocity potential is given by

$$\phi(r', t') = \int_0^\infty \tilde{g}(\xi) \sin(\xi t') J_0(\xi r') \, d\xi, \tag{B6}$$

where J_0 is the Bessel function of order zero. Substituting (B6) into (B3) it is readily found that in terms of the physical variables the initial conditions are

$$t' = 0, \qquad u = v = 0, \qquad p = \rho = g(r'). \tag{B7}$$

Of interest to the direct numerical simulation in Section 8 is a Gaussian initial pressure distribution. For this case the full solution in the stationary frame of reference may be written as

$$t = 0, \qquad u = v = 0, \qquad p = \rho = \varepsilon_1 e^{-\alpha_1 r'^2} \tag{B8}$$

$$u(x, y, t) = \frac{\varepsilon_1 (x - Mt)}{2\alpha_1 \eta} \int_0^\infty e^{-\xi^2/4\alpha_1} \times \sin(\xi t) J_1(\xi\eta) \, \xi \, d\xi \tag{B9}$$

$$v(x, y, t) = \frac{\varepsilon_1 y}{2\alpha_1 \eta} \int_0^\infty e^{-\xi^2/4\alpha_1} \times \sin(\xi t) J_1(\xi\eta) \, \xi \, d\xi \tag{B10}$$

$$p(x, y, t) = \rho = \frac{\varepsilon_1}{2\alpha_1} \int_0^\infty e^{-\xi^2/4\alpha_1} \times \cos(\xi t) J_0(\xi\eta) \, \xi \, d\xi, \tag{B11}$$

where $\eta = [(x - Mt)^2 + y^2]^{1/2}$ and J_1 is the Bessel function of order one. The parameter α_1 is related to the half-width of the Gaussian, b, by $\alpha_1 = \ln 2/b^2$.

B2. *Entropy Waves*

In the moving coordinate system a family of entropy wave solutions is given by

$$p = u = v = 0, \qquad \rho = \Psi(x', y'), \tag{B12}$$

where Ψ is arbitrary. If the initial distribution is Gaussian the full solution in the stationary coordinate system is

$$p = u = v = 0, \qquad \rho = \varepsilon_2 e^{-\alpha_2[(x - Mt)^2 + y^2]}. \tag{B13}$$

B3. *Vorticity Waves*

In the moving coordinate system a family of vorticity waves is given by the time independent solutions of

$$\nabla' \cdot \mathbf{v} = 0, \qquad \rho = p = 0. \tag{B14}$$

Suppose the initial velocity distribution is

$$t = 0, \quad u = \varepsilon_3 y' e^{-\alpha_3 r'^2}, \quad v = -\varepsilon_3 x' e^{-\alpha_3 r'^2}. \tag{B15}$$

It is easy to check that (B15) satisfies (B14). The full solution in the stationary frame of reference is

$$\begin{aligned} p &= \rho = 0 \\ u &= \varepsilon_3 y e^{-\alpha_3[(x - Mt)^2 + y^2]} \\ v &= -\varepsilon_3 (x - Mt) e^{-\alpha_3[(x - Mt)^2 + y^2]}. \end{aligned} \tag{B16}$$

ACKNOWLEDGMENTS

This work was supported by the NASA Lewis Research Center Grant NAG 3-1267 and in part by the office of Naval Research Grant No. N00014-89-J-1836 and the Florida State University through time granted on its Cray-YMP supercomputer.

REFERENCES

1. R. W. MacCormack, AIAA Paper 69-0354, 1969.
2. R. M. Beam and R. F. Warming, *AIAA J.* **16**, 393 (1978).
3. J. L. Steger and R. F. Warming, *J. Comput. Phys.* **40**, 263 (1981).
4. A. Jameson, W. Schmidt, and E. Turkel, AIAA Paper 81-1259, 1981.
5. P. Roe, *J. Comput. Phys.* **43**, 356 (1981).
6. S. Osher and F. Solomon, *Math. Comput.* **38**, 339 (1982).
7. A. Harten, *J. Comput. Phys.* **49**, 357 (1983).
8. S. Osher and S. Chakravarthy, *SIAM J. Numer. Anal.* **21**, 955 (1984).
9. P. K. Sweby, *SIAM J. Numer. Anal.* **21**, 995 (1984).
10. G. B. Whitham, *Linear and Nonlinear Waves* (Wiley-Interscience, New York, 1974).
11. A. Bayliss and E. Turkel, *Commun. Pure Appl. Math.* **33**, 107 (1980).
12. A. Bayliss and E. Turkel, *J. Comput. Phys.* **48**, 182 (1982).
13. B. Engquist and A. Majda, *Math. Comput.* **31**, 627 (1977).
14. B. Engquist and A. Majda, *Commun. Pure Appl. Math.* **32**, 313 (1979).
15. R. L. Higdon, *Math. Comput.* **47**, 437 (1986).
16. R. L. Higdon, *Math. Comput.* **49**, 65 (1987).
17. H. Jiang and Y. S. Wong, *J. Comput. Phys.* **88**, 205 (1990).
18. R. Kosloff and D. Kosloff, *J. Comput. Phys.* **63**, 363 (1986).
19. K. W. Thompson, *J. Comput. Phys.* **68**, 1 (1987).
20. K. W. Thompson, *J. Comput. Phys.* **89**, 439 (1990).
21. C. K. W. Tam and J. C. Webb, *J. Comput. Phys.*, submitted.
22. R. Vichnevetsky, *Math. Comput. Simul.* **22**, 98 (1980).
23. R. Vichnevetsky and J. B. Bowles, *Fourier Analysis of Numerical Approximations of Hyperbolic Equations* (SIAM, Philadelphia, 1982).
24. L. N. Trefethen, *SIAM Rev.* **24**, 113 (1982).
25. C. K. W. Tam, AIAA J. **30**, 608 (1992).
26. S. K. Lele, Center for Turbulence Research Manuscript 107, NASA Ames Research Center/Stanford University, 1990 (unpublished).